

Long-term incubations provide insight into the mechanisms of anaerobic oxidation of methane in methanogenic lake sediments

Hanni Vigderovich^a, Werner Eckert^b, Michal Elul^a, Maxim Rubin-Blum^c, Marcus Elvert^d, Orit Sivan^a

^a Department of Earth and Environmental Science, Ben-Gurion University of the Negev, Beer Sheva, Israel

^b Israel Oceanographic & Limnological Research, The Yigal Allon Kinneret Limnological Laboratory, Israel

^c Israel Oceanographic & Limnological Research, Haifa, Israel

^d MARUM - Center for Marine Environmental Sciences and Faculty of Geosciences, University of Bremen, Bremen, Germany

Corresponding author: Hanni Vigderovich, hannil@post.bgu.ac.il

Abstract

Anaerobic oxidation of methane (AOM) is among the main processes limiting the release of the greenhouse gas methane from natural environments. Geochemical profiles and experiments with fresh sediments from Lake Kinneret (Israel) indicate that iron-coupled AOM (Fe-AOM) sequesters 10-15% of the methane produced in the methanogenic zone (> 20-cm sediment depth). The oxidation of methane in this environment was shown to be mediated by a combination of *mcr* gene-bearing archaea and *pmoA* gene-bearing aerobic bacterial methanotrophs. Here, we used sediment slurry incubations under controlled conditions to elucidate the electron acceptors and microorganisms that are involved in the AOM process over the long-term (~18 months). We monitored the process with the addition of ¹³C-labeled methane and two stages of incubations: (i) enrichment of the microbial population involved in AOM and (ii) slurry dilution and manipulations, including the addition of several electron acceptors (metal oxides, nitrate, nitrite and humic substances) and inhibitors (2-bromoethanesulfonate, acetylene and sodium molybdate) of methanogenesis, methanotrophy and sulfate reduction/sulfur disproportionation. Carbon isotope measurements in the dissolved inorganic carbon pool suggest the persistence of AOM, consuming 3-8% of the methane produced at a rate of 2.0±0.4 nmol g⁻¹ dry sediment day⁻¹. Lipid carbon isotopes and metagenomic analyses point towards methanogens as the sole microbes performing the AOM process by reverse methanogenesis. Humic substances and iron oxides, but not sulfate, manganese, nitrate, or nitrite, are the likely electron acceptors used for this AOM. Our observations support the contrast between methane oxidation mechanisms in naturally anoxic lake sediments, with potentially co-existing aerobes and anaerobes, and long-term incubations, wherein anaerobes prevail.

Keywords: Anaerobic oxidation of methane (AOM), lake sediments, dissolved inorganic carbon, stable carbon isotopes, electron acceptors, archaea, methanogens, methanotrophs, lipids.

34

35 **1. Introduction**

36 Methane (CH₄) is an important greenhouse gas (Wuebbles and Hayhoe, 2002), which has both
37 anthropogenic and natural sources, the latter of which account for about 50% of the emission of this gas
38 to the atmosphere (Saunois et al., 2020). Naturally occurring methane is mainly produced biogenically
39 via the methanogenesis process, which is performed by methanogenic archaea. Traditionally
40 acknowledged as the terminal process anchoring carbon remineralization (Froelich et al. 1979),
41 methanogenesis occurs primarily via the reduction of carbon dioxide by hydrogen in marine sediments
42 and via acetate fermentation in freshwater systems (Whiticar et al. 1986).

43 Methanotrophy, the aerobic and anaerobic oxidation of methane (AOM) by microbes, naturally controls
44 the release of this gas to the atmosphere (Conrad, 2009; Reeburgh, 2007; Knittel and Boetius, 2009). In
45 marine sediments, up to 90% of the upward methane flux is consumed anaerobically by sulfate, and in
46 established diffusive profiles, that methane consumption occurs within a distinct sulfate-methane
47 transition zone (Valentine 2002). While sulfate-dependent AOM, catalyzed by the archaeal ANaerobic
48 MEthanotrophs (ANMEs) 1-3, is widespread chiefly in marine sediments (Hoehler et al., 1994; Boetius
49 et al., 2000; Orphan et al., 2001; Treude et al., 2005, 2014), methane oxidation in other environments
50 can be coupled to other electron acceptors (e.g. Raghoebarsing et al., 2006; Ettwig et al. 2010; Sivan et
51 al., 2011; Crowe et al. 2011; Norði and Thamdrup 2014; Valenzuela et al., 2017).

52 In freshwater sediments, sulfate is often depleted, and methanogenesis may be responsible for most of
53 the organic carbon remineralization, resulting in ~~thus~~ high concentrations of methane in shallow
54 sediments (Sinke et al., 1992). Indeed, lakes and wetlands, are responsible for 33-55% of naturally
55 emitted methane (Rosentreter et al., 2021). A large portion of this produced methane is oxidized by
56 aerobic (type I, ~~type II and type X~~) methanotrophic bacteria via oxygen. Aerobic methanotrophy is
57 generally observed in the sediment-water interface (Damgaard et al. 1998) and/or in the water column
58 thermocline (Bastviken 2009). AOM, however, can also consume over 50% of the produced methane
59 (Segarra et al. 2015).

60 Sulfate can be an electron acceptor of AOM in freshwater sediments, as was shown for example in Lake
61 Cadagno (Schubert et al., 2011, Su et al., 2020). Alternative electron acceptors for AOM in natural
62 freshwater environments and cultures include humic substances, nitrate, nitrite and metals (such as iron
63 manganese and chromium). Natural humic substances and their synthetic analogs were shown to
64 function as terminal electron acceptors for AOM in soils, wetlands and cultures (Valenzuela et al., 2017;
65 2019; Bai et al., 2019; Zhang et al., 2019; Fan et al., 2020). Nitrate-dependent AOM has been
66 demonstrated in a consortium of archaea and denitrifying bacteria from a canal (Raghoebarsing et al.,
67 2006), in freshwater lake sediments (Norði and Thamdrup 2014) and ~~in~~ a sewage enrichment culture of
68 ANME-2d (Haroon et al., 2013; Arshad et al., 2015). Nitrite is exploited to oxidize methane by the

69 aerobic bacteria *Methyloirabilis* (NC-10), which split the nitrite to N₂ and O₂ and then uses the
70 produced oxygen to oxidize the methane (Ettwig et al., 2010). ANME-2d were also suggested to be
71 involved in Cr(VI) coupled AOM, either alone or with a bacterial partner (Lu et al., 2016). Iron and/or
72 manganese coupled AOM have also been suggested in lakes (Sivan et al., 2011; Crowe et al. 2011;
73 Norđi et al., 2013), sometimes by supporting sulfate-coupled AOM (Shubert et al., 2011; Su et al., 2020;
74 Mostovaya et al., 2021). Iron-coupled AOM was also shown to occur in enriched, denitrifying cultures
75 from sewage where it was performed by ANME-2 (Ettwig et al. 2016), and in a bioreactor with natural
76 sediments (Cai et al., 2018).

77 The mechanism and role of iron-coupled AOM in lake sediments have been studied with a variety of
78 tools in the sediments of Lake Kinneret. *In-situ* pore water profiles and top core experiments (Sivan et
79 al., 2011), diagenetic models (Adler et al., 2011) and batch incubation experiments with fresh sediment
80 slurries (Bar-Or et al., 2017) suggest that iron coupled-AOM (Fe-AOM) removes 10-15% of the
81 produced methane in the deeper part of the methanogenic zone (> 20 cm below the water-sediment
82 interface). Analysis of the microbial community structure suggested that both methanogenic archaea
83 and methanotrophic bacteria are potentially involved in methane oxidation (Bar-Or et al., 2015).
84 Analyses of stable isotopes in fatty acids, 16S rRNA gene amplicons and metagenomics showed that
85 both reverse methanogenesis by archaea and bacterial type I aerobic methanotrophy by
86 Methylococcales play important role in methane cycling (Bar-Or et al., 2017; Elul et al., 2021). Aerobic
87 methanotrophy, which has also been observed in the hypolimnion and sediments of several other lakes
88 that are considered anoxic (Beck et al., 2013; Oswald et al., 2016; Martinez-Cruz et al., 2017; Cabrol
89 et al., 2020), may be driven by the presence of oxygen at nanomolar levels (Weng et al., 2018). Pure
90 cultures of the ubiquitous aerobic methanotrophs Methylococcales have indeed been shown to survive
91 under hypoxia conditions either by oxidizing methane and with nitrate (Kits et al., 2015), by switching
92 to iron reduction (Zheng et al., 2020), or even by exploiting their methanobactins to generate their own
93 oxygen to fuel their methanotrophic activity (Dershwitz et al., 2021). The latter study also showed that
94 the alphaproteobacterial methanotroph *Methylocystis* sp., strain SB2, can couple methane oxidation and
95 iron reduction. However, whether these aerobic methanotrophic bacteria are able to oxidize methane
96 under strictly anoxic conditions and which electron acceptors are available to facilitate that activity are
97 still not known.

98 In the current study, we used long-term anaerobic incubations to assess the dynamics of methane-
99 oxidizing microbes under anoxic conditions and to quantify the respective availabilities of different
100 electron acceptors for AOM. To that end, we diluted fresh methanogenic sediments from Lake Kinneret
101 with original porewater from the same depth and amended the sediment with ¹³C-labeled methane. Our
102 experiment design comprised of two stages, the first of which included the enrichment of the microbial
103 population involved in AOM, while the second involved an additional slurry dilution and several
104 manipulations with different electron acceptors and inhibitors. We measured methane oxidation rates

(based on ^{13}C -DIC enrichment), determined the characteristics of each electron acceptor (via its turnover), and evaluated changes in microbial diversity over various incubation periods (based on metagenomics and lipid biomarkers). The results from the long-term anaerobic incubations were compared to those of batch and semi-continuous bioreactor experiments.

2. Methods

2.1 Study site

Lake Kinneret (Sea of Galilee) is a warm, monomictic, freshwater lake that is 21 km long and 13 km wide and located in northern Israel. Its maximum depth is ~42 m at its center (station A, Figure S1) while its average depth is 24 m. From March to December, the lake is thermally stratified, and from April to December, the hypolimnion is anoxic. Surface water temperatures range from 15°C in the winter (January) to 32°C in the summer (August), while the lake's bottom water temperatures remain in the range of 14-17°C throughout the year. The sediment from the deep methanogenic zone used in this study (sediment samples taken from a sediment depth of ~20 cm from the water-sediment interface at the lake's center) contains 50% carbonates, 30% clay and 7% iron (Table S1). The dissolved organic carbon (DOC) concentration of the porewater increases with depth, ranging from ~6 mg C L⁻¹ at the sediment-water interface to 17 mg C L⁻¹ at a depth of 25 cm (Adler et al., 2011). The concentrations of dissolved methane in the sediment porewater increase sharply with sediment depth, reaching a maximum of more than 2 mM at a depth of 15 cm, after which the amounts of dissolved methane gradually decreased with depth to 0.5 mM at a depth of 30 cm (Adler et al., 2011; Sivan et al., 2011; Bar-Or et al., 2015).

2.2 Experimental setup

2.2.1 General

In this study we compared three incubation strategies (A, B and C; Fig. 1) in Lake Kinneret methanogenic sediments (sediment depths > 20 cm), which were amended with original porewater from the same depth, ^{13}C -labeled methane (0.05-2 ml; Table 1), different potential electron acceptors for AOM (nitrite, nitrate, iron and manganese oxides and humic substances) and activity inhibitors. We inhibited the *mcr* gene with 2-bromoethanesulfonate (BES), methanogenesis and methanotrophy with acetylene, and sulfate reduction and sulfur disproportionation with Na-Molybdate (Nollet et al., 1997; Oremland & Capone, 1988; Lovley & Klug, 1983). Below we describe the three incubation strategies (Fig. 1).

A) Long-term, two-stage slurry incubations with a 1:1 sediment to porewater ratio and high methane content for the first three months (first stage) to ensure the enrichment of the microorganisms involved in AOM. After three months, the slurry was diluted with porewater to a 1:3 ratio (second stage) and

different reactants were added to the incubations, which were subsequently monitored for up to 18 months.

B) Semi-continuous bioreactor experiments in which sediments were collected up to three days before the experiment was set up (freshly sampled sediments). ~~The~~ sediment to porewater ratio ~~of was~~ 1:4 ~~and, where~~ porewater was exchanged regularly.

C) Batch incubation experiments with freshly sampled sediments and porewater at a 1:5 ratio, respectively, and amended with hematite. This experimental set-up was described in our previous studies (Bar-Or et al., 2017; Elul et al., 2021).

The sediments for the slurries conducted in the current work were collected during seven day-long sampling campaigns aboard the research vessel *Lillian* between 2017 and 2019 from the center of the lake (Station A, Fig. S1) using a gravity corer with a 50-cm Perspex core liner. The length of the sediment in each core was 35-45 cm. During each sampling campaign, 1-2 sediment cores were collected for the incubations and 10 cores were collected for the porewater extraction. Sediments from the deeper methanogenic zone (sediment depths > 20 cm) for the experiments were diluted with porewater from the methanogenic zone of parallel cores sampled on the same day. The bottom part of the sediment cores (below 20 cm) was transferred, as a bulk, to a dedicated 5 L plastic container onboard. The cores and the container were brought back to the lab, where the cores were kept at 4°C, and tThe porewater was extracted on the same day of sampling. ~~The sediment cores were sliced while onboard, and sediment samples from the methanogenic zone (> 20 cm) were transferred to a dedicated container.~~ In the lab, sediments were collected from the container with 20-ml cutoff syringes and moved to 50-ml falcon tubes. The porewater was extracted by centrifugation at 9300 g for 15 min at 4°C, syringe filtered by 0.22-µm filters into 250-ml pre-autoclaved glass bottles, crimp-sealed with rubber stoppers, and flushed for 30 min with N₂. The extracted porewater was kept under anaerobic conditions at 4°C until its use. The sediments for the incubations were subsampled ~~ds~~ from the liners and diluted no later than three days after their collection from the lake and treated further according to the experimental strategies described above (setup A or B).

2.2.2 Experiment type A set-up: Long-term two-stage incubations (henceforth referred to as “two-stage” for simplicity)

Experiment A comprised ten two-stage incubation experiments (experiment serial numbers (SN) 1-10; Table 1) with different treatments (electron acceptors/shuttling/inhibitors). In the first stage (pre-incubation slurry), the sediment core was sliced under continuous N₂ flushing a N₂-atmosphere and sediments from depths > 20 cm were collected into zipper bags. The sediment was homogenized by shaking the sediment in the bag, and between 80-100 gr was transferred into 250-ml glass bottles under continuous N₂ flushing. The sediments were diluted with the extracted porewater to create a 1:1 sediment to porewater slurry with a headspace of 70-90 ml (Fig. 1). The slurries were sealed with rubber

173 stoppers and crimped caps and were flushed with N₂ (99.999%, MAXIMA, Israel) for 30 min. Methane
174 (99.99%, MAXIMA, Israel) was injected using a gas-tight syringe for a final content of 20% in the
175 headspace, where 10% of the injected methane was ¹³C-labeled methane (99%, Sigma-Aldrich). When
176 significant AOM activity was observed based on the increase of δ¹³C_{DIC} after approximately three
177 months (Fig. S2), some of the incubations were further diluted during the second stage of the
178 experiments. The remainder of the incubations continued to be run with porewater exchange while the
179 δ¹³C_{DIC} values were monitored every three months.

180 All the experiments were set up similarly (see dates and detailed protocols in the supplementary
181 information): the pre-incubation bottle was opened and subsamples (~18 g each) were transferred with
182 a syringe and a Tygon® tube under a laminar hood and continuous flushing of N₂ gas into 60-ml glass
183 bottles. The subsamples were then diluted with fresh anoxic porewater from the methanogenic zone (as
184 described above) to achieve a 1:3 sediment to porewater ratio (Fig. 1) while leaving 24 ml of headspace
185 in each bottle. The bottles were crimp-sealed, flushed with N₂ gas for 5 min, shaken vigorously and
186 flushed again (3 times). Then ¹³C-labeled methane was added to all of the bottles as described in Table
187 1. The "killed" control slurries in each experiment were autoclaved twice and cooled, only after which
188 they were amended with the appropriate treatments and ¹³C-labeled methane.

189 To the diluted (1:3) batch slurries electron acceptors were added either as a powder (hematite –
190 experiment no. 1, magnetite – experiment no. 2, clay and humic substances – experiment no. 7, MnO₂
191 – experiment no. 3) or in dissolved form in double-distilled water (DDW) (KNO₃ – experiment no. 4,
192 NaNO₂ – experiment no. 5). In addition, the potential involvement of sulfur cycling in the transfer of
193 electrons was tested in experiment no. 2 via its inhibition with Na-molybdate (Lovley and Klug, 1983).
194 The synthetic analog for humic substances, i.e., 9,10-anthraquinone-2,6-disulfonate (AQDS), was
195 dissolved in DDW (detailed in the supplementary information) and added to the bottles of experiment
196 no. 6 until a final concentration of 5 mM was achieved in each bottle. Amorphous iron (Fe(OH)₃) was
197 prepared in the lab by dissolving FeCl₃ in DDW that was then titrated with NaOH 1.5 N up to pH 7 and
198 injected into the bottles of experiment no. 2-. The final concentration of each addition is detailed in
199 Table 1. The ¹³C-labeled methane was injected into all of the experimental bottles at the beginning of
200 each experiment (unless described otherwise) by using a gas-tight syringe from a stock bottle filled with
201 ¹³C-labeled methane gas (which was replaced with saturated NaCl solution). Three different inhibitors
202 were added to three different experiments: Molybdate was added to experiment No. 1 (to one bottle of
203 methane-only treatment, magnetite treatment and amorphous iron treatment) to detect the feasibility of
204 an active sulfur cycle; BES was added to experiment No. 8 at the start of the experiment; and acetylene
205 was added to experiment No. 9, wherein it was injected during the experiment into two bottles at
206 different timepoints after ¹³C enrichment was observed in the DIC (Table 1).

All live treatments were set up in duplicate or triplicate, depending on the amount of the pre-incubated slurry aimed for each experiment, and the results are presented as the average with an error bar. In two experiments, only one "killed" control bottle was set up, and the remainder of the slurry was prioritized for other treatments, because the killed controls repeatedly showed no activity in several previous experiments. The humic substrate experiment used a natural (humic) substance that was extracted from a lake near Fairbanks, Alaska, where ~~the~~ iron reduction was observed in the methanogenic zone. One experiment was set up without any additional electron acceptor to assess the rate of methanogenesis in the two-stage slurries. Porewater was sampled anaerobically for $\delta^{13}\text{C}_{\text{DIC}}$ and dissolved Fe(II) measurements in duplicate (2 ml), and methane was measured from the headspace. Variations in the $\delta^{13}\text{C}_{\text{DIC}}$ values between the experiments resulted from different amounts of ^{13}C -labeled methane injected at the start of each experiment (geochemical measurements detailed in the analytical methods section below).

2.2.3 Experiment type B setup: Semi-continuous bioreactor

Semi-continuous bioreactors were used to monitor the redox state regularly at close-to-natural *in-situ* conditions for 15 months in freshly collected sediments. Two 0.5-L semi-continuous bioreactors (Fig. 1) (LENZ, Weinheim, Germany) were set up with freshly sampled sediments from the methanogenic zone (25 - 40 cm) and extracted porewater from the same depth from Station A on Lake Kinneret immediately after their collection. Both reactors were filled, headspace-free, with a slurry at a 1:4 sediment to porewater ratio. One bioreactor was amended with 10 mM hematite while the second, which was a control, was not amended. To dissolve ^{13}C -labeled methane in the porewater, 15 ml of porewater were replaced with 15 ml of methane gas (13 ml of $^{12}\text{CH}_4$ and 2 ml of $^{13}\text{CH}_4$) to produce a methane-only headspace for 24 h, during which time the reactors were shaken repeatedly. After 24 h, the gas was replaced with anoxic porewater, thus eliminating the headspace, which resulted in lower methane concentrations (0.2 mM) than in either the two-stage incubations or the fresh batch experiment (~2 mM). The redox potential was monitored continuously using a platinum/glass electrode (Metrohm, Herisau, Switzerland) to verify anoxic conditions and to determine the redox state throughout the incubation period. The bioreactors were subsampled weekly to bi-weekly, and the sample volume (5-10 ml) was replaced immediately by preconditioned anoxic (flushed with N_2 gas for 15 min) porewater from the methanogenic zone. As outlined below, samples were analyzed for dissolved Fe(II), methane and $\delta^{13}\text{C}_{\text{DIC}}$. Additional subsamples for metagenome and lipid analyses were taken at the beginning of the experiment and on days 151 and 382, respectively.

2.2.4 Experiment type C setup: Fresh batch experiment

Sediments for this experiment were collected in August 2013 at Station A using a protocol similar to that used to collect the sediments for the pre-incubations. Sediments from depths greater than 26 cm were diluted under anaerobic conditions with porewater from the same depth to obtain a ratio of

sediment to porewater of 1:5. The resulting slurry was then divided between 60-ml glass bottles (40 ml slurry in each bottle). The sampling and experimental setup are described in detail in our earlier study (Bar-Or et al., 2017). Here we present our results of the $\delta^{13}\text{C}_{\text{DIC}}$, metagenome and lipid analyses of two treatments: natural (with only ^{13}C -labeled methane) and hematite. The experiment ran for 15 months.

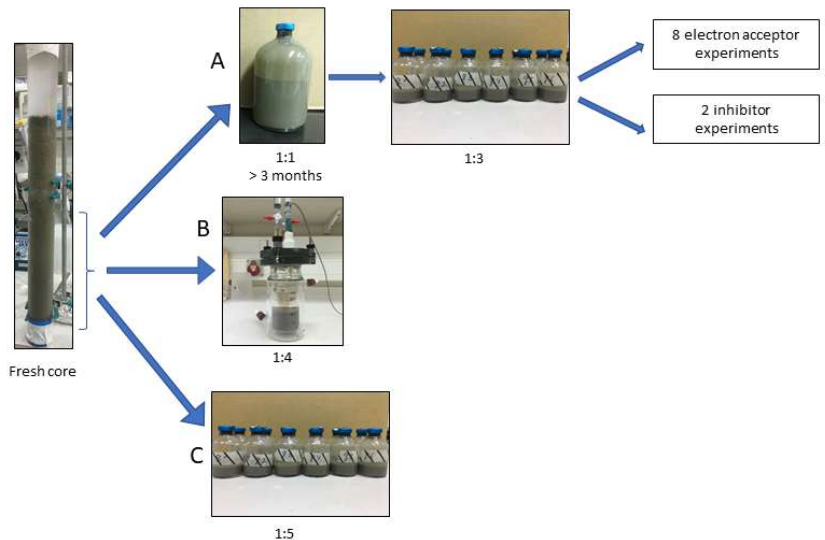


Figure 1: Flow diagram of the experimental design. Three types of experiments were set up to investigate the methanogenic zone sediments (deeper than 20 cm): **A)** Two-stage slurry experiments, with 1:1 ratio of sediment to porewater incubations and then with diluted pre-incubated slurries and porewater (1:3 ratio of sediment to porewater). **B)** Semi-aerobic-continuous bioreactor experiment with freshly collected sediment. **C)** Fresh batch experiment – slurry experiment with freshly collected sediments (Bar-Or et al., 2017).

Table 1: Details of the three types of experiments: two-stage, semi-aerobic bioreactor and fresh batch experiments.

Experiment serial number (SN)	Experiment	Treatment	# of bottles	CH ₄ [mL]	¹³ CH ₄ [mL]	Fe ₂ O ₃ [mM]	Fe ₂ O ₄ [mM]	Fe(OH) ₃ [mM]	MnO ₂ [mM]	NO ₂ ⁻ [mM]	NO ₃ ⁻ [mM]	AQDS [mM]	Humic substances [mM]	PCA[mM]	Fe-bearing montmorillonite (clay) [g]	Na ₂ S ₂ O ₄ [mM]	BES [mM]	Acetylene [μL]	Temp [°C]	Duration [day]	Comments
1	Hematite	¹³ CH ₄ 13C44+hematite	2		1	10													20	201	The methane that was added at the beginning of the experiment was not labelled, so ¹³ C-labelled methane was added after 105 days. Na ₂ S ₂ O ₄ was added to one of the bottles on day 365
2	Magnetite	¹³ CH ₄ ¹³ CH ₄ +magnetite ¹³ CH ₄ +Fe(OH) ₃ Killed+ ¹³ CH ₄ +magnetite	2 2 2 1		1 1 1 1		10	10								1 1 1			16 16 16	447	Na ₂ S ₂ O ₄ was added to one of the bottles on day 365
3	MnO ₂	¹³ CH ₄ ¹³ CH ₄ +MnO ₂	2 2		1.2 1.2			10											20	201	200 μL ¹³ CH ₄ was added on day 1, then another 1 mL was added on day 24
4	Nitrate	¹³ CH ₄ +NO ₃ ⁻ (high conc.) ¹³ CH ₄ +hematite ¹³ CH ₄ +NO ₃ ⁻ (high conc.)+hematite ¹³ CH ₄ +NO ₃ ⁻ (low conc.)+hematite Killed+ ¹³ CH ₄ +NO ₃ ⁻ (high conc.)+hematite	2 2 2 2 1	1 1 1 1 1	0.5 0.5 0.5 0.5 0.5	12 12 12 12 12					1 1 0.2 1								20 20 20 20	306	
5	Nitrite	¹³ CH ₄ ¹³ CH ₄ +NO ₂ ⁻ (high conc.)+hematite ¹³ CH ₄ +NO ₂ ⁻ (low conc.)+hematite Killed+ ¹³ CH ₄ +NO ₂ ⁻ (high conc.)+hematite	3 2 2 2	1 1 1 1	0.5 0.5 0.5 0.5				0.5 0.1 0.5										20 20 20	493	
6	AQDS	¹³ CH ₄ ¹³ CH ₄ +AQDS ¹³ CH ₄ +AQDS+hematite Killed+ ¹³ CH ₄ +AQDS	3 2 2 2	1 1 1 1								5 5							20 20 20	264	
7	Natural humic acids and clay	¹³ CH ₄ ¹³ CH ₄ +hematite ¹³ CH ₄ +humic acid ¹³ CH ₄ +clay Killed+ ¹³ CH ₄ +hematite	2 2 2 2		1 1 1 1								0.5						20 20 20	169	The head space of the experiment bottles was flushed with N ₂ on day 51 and ¹³ CH ₄ was added. This was done in order to match the clay bottles.
8	Biomethanogenesis (BES)	¹³ CH ₄ +hematite ¹³ CH ₄ +hematite+BES ¹³ CH ₄ +hematite	2 2 4	9 9 1	1 1 0.5	10 10 10													20 20 20	493	
9	Acetylene	¹³ CH ₄ +hematite+acetylene Killed+ ¹³ CH ₄ +hematite No additions	2 2 3	1 1 1	0.5 0.5 1	10 10 10													20 20 20	321	Acetylene was injected to each bottle at different time points during the experiment
10	No electron acceptor	¹³ CH ₄ ¹³ CH ₄ ¹³ CH ₄ +hematite	3 13 13		1 2 2														16 16	345	
	Semi-bioreactor	¹³ CH ₄ +hematite			0.05	20													20	677	
	Freshly collected sediment exp.	¹³ CH ₄ +hematite			0.05	20													20	467	

2.3 Analytical methods

Experiment serial number (SN)	Experiment	Treatment	# of bottles	CH ₄ [mM]	¹³ CH ₄ [mM]	Fe ₂ O ₃ [mM]	Fe(OH) ₃ [mM]	MnO ₂ [mM]	NO ₂ ⁻ [mM]	NO ₃ ⁻ [mM]	AQDS [mM]	Humic substances [mM]	PCA [mM]	Fe-bearing nontronite [clay] [g]	Na ₂ -molybdate [mM]	BES [mM]	Acetylene [μL]	Temp [°C]	Duration [day]	Comments	
1	Hematite	¹³ CH ₄	2		1													20	201		
		¹³ CO ₂ +Hematite	2		1	10												20		The methane that was added at the beginning of the experiment was not labeled, so ¹³ C-labeled methane was added after 105 days. Na ₂ -molybdate was added to one of the bottles on day 365	
2	Magnetite	¹³ CH ₄	2	1												1		16	447		
		¹³ CH ₄ -magnetite	2	1	10											1		16			
		¹³ CH ₄ +Fe(OH) ₃	2	1														16			
		Killed+ ¹³ CH ₄ -magnetite	1	1	10													16			
3	MnO ₂	¹³ CH ₄	2	1.2														20	201	200 μL ¹³ CH ₄ was added on day 1, then another 1 mL was added on day 24, another 1 mL was added on day 1, then another 1 mL was added on day 24,	
		¹³ CH ₄ +MnO ₂	2	1.2			10											20			
4	Nitrate	¹³ CH ₄ +NO ₂ (high conc.)	2	1	0.5	12			1										20		
		¹³ CH ₄ -hematite	2	1	0.5	12												20			
		¹³ CH ₄ +NO ₂ (high conc.)+hematite	2	1	0.5	12				1								20	306		
		¹³ CH ₄ +NO ₂ (low conc.)+hematite	2	1	0.5	12				0.2								20			
		Killed+ ¹³ CH ₄ +NO ₂ (high conc.)+hematite	1	1	0.5	12				1								20			
5	Nitrite	¹³ CH ₄	3	1	0.5														20		
		¹³ CH ₄ +NO ₂ (high conc.)+hematite	2	1	0.5	10			0.5									20	493		
		¹³ CH ₄ +NO ₂ (low conc.)+hematite	2	1	0.5	10			0.1									20			
		Killed+ ¹³ CH ₄ +NO ₂ (high conc.)+hematite	2	1	0.5	10			0.5									20			
		¹³ CH ₄	3	1														20			
6	AQDS	¹³ CH ₄ +AQDS	2	1							5							20	264		
		¹³ CH ₄ +AQDS+hematite	2	1	10						5							20			
		Killed+ ¹³ CH ₄ +AQDS	2	1														20			
7	Natural humic acids and clay	¹³ CH ₄	2		1													20			The head space of the experiment bottles was flushed with N ₂ on day 51 and ¹³ CH ₄ was added. This was done to match the the clay bottles.
		¹³ CH ₄ -hematite	2	1	10													20	169		
		¹³ CH ₄ -humic acid	2		1								0.5					20			
		¹³ CH ₄ +clay	2	1												1		20			
		Killed+ ¹³ CH ₄ -hematite	2	1	10													20			
8	Bromothanesulfonate (BES)	¹³ CH ₄ -hematite	2	9	1	10												20	493		
		¹³ CH ₄ -hematite+BES	2	9	1	10											20				
9	Acetylene	¹³ CH ₄ -hematite	4	1	0.5	10											120	20	321	Acetylene was injected to each bottle at different time points during the experiment.	
		¹³ CH ₄ -hematite+acetylene	2	1	0.5	10												20			
10	No electron acceptor	Killed+ ¹³ CH ₄ -hematite	2	1	0.5	10												20	147		
		No additions	3		1													20			
	Semi-bioreactor	¹³ CH ₄		15														16	345		
		¹³ CH ₄ -hematite		15	10													16	677		
	Freshly collected sediment exp.	¹³ CH ₄ -hematite		0.05	20													20	467		

2.3.1 Geochemical measurements

Measurements of $\delta^{13}\text{C}_{\text{DIC}}$ were performed on a DeltaV Advantage Thermo Scientific isotope-ratio mass-spectrometer (IRMS). Results are reported referent to the Vienna Pee Dee Belemnite (VPDB) standard. For these measurements, about 0.3 ml of filtered (0.22 μm) porewater was injected into a 12-ml glass vial with a He atmosphere and 10 μl of H_3PO_4 85% to acidify all the DIC species to CO_2 (g). The headspace autosampler (CTC Analytics; Type PC PAL) sampled the gas from the vials and measured the $\delta^{13}\text{C}_{\text{DIC}}$ of the sample on the GasBench interface with a precision of ± 0.1 ‰. DIC was measured on the IRMS using the peak height and a precision of 0.05 mM. Dissolved Fe(II) concentrations were determined using the ferrozine method (Stookey, 1970) by ~~a-spectrophotometer-HANON i2 visible spectrophotometer~~ at a 562-nm wavelength with a detection limit of 1 $\mu\text{mol L}^{-1}$. A 100- μL headspace sample was taken for methane measurements with a gas-tight syringe and was analyzed by gas chromatograph (Focus GC, Thermo) equipped with a flame ionization detector (FID) and a packed column (Shincarbon ST) with a helium carrier gas (UHP) and a detection limit of 1 nmol methane. Bottles to which acetylene was added were also measured by the GC with the same column and carrier gas for ethylene to determine the acetylene turnover with the N cycle.

2.3.2 Lipid analysis

A sub-set of samples (Table 3) was investigated for the assimilation of ^{13}C -labeled methane into polar lipid-derived fatty acids (PLFAs) and intact ether lipid-derived hydrocarbons. A total lipid extract (TLE) was obtained from 0.4 to 1.6 g of the freeze-dried sediment or incubated sediment slurry using a modified Bligh and Dyer protocol (Sturt et al., 2004). Before extraction, 1 μg of 1,2-diheneicosanoyl-*sn*-glycero-3-phosphocholine and 2-methyloctadecanoic acid were added as internal standards. PLFAs in the TLE were converted to fatty acid methyl esters (FAMES) using saponification with KOH/MeOH and derivatization with BF_3/MeOH (Elvert et al., 2003). Intact archaeal ether lipids in the TLE were separated from the apolar archaeal lipid compounds using preparative liquid chromatography (Meador et al., 2014) followed by ether cleavage with BBr_3 in dichloromethane forming hydrocarbons (Lin et al., 2010). Both FAMES and ether-cleaved hydrocarbons were analyzed by GC-mass spectrometry (GC-MS; Thermo Finnigan Trace GC coupled to a Trace MS) for identification and by GC-IRMS (Thermo Scientific Trace GC coupled via a GC Isolink interface to a Delta V Plus) to determine $\delta^{13}\text{C}$ values by using the column and temperature program settings described by Aepfler et al. (2019). The $\delta^{13}\text{C}$ values are reported with an analytical precision better than 1‰ as determined by long-term measurements of an *n*-alkane standard with known isotopic composition of each compound. Reported fatty acid isotope data are corrected for the introduction of the methyl group during derivatization by mass balance calculation similar to equation 1 (see below) using the measured $\delta^{13}\text{C}$ value of each FAME and the known isotopic composition of methanol as input parameters.

2.3.3 Metagenomic analysis

For the metagenomic analyses, total genomic DNA was extracted from the semi-aerobic bioreactor with hematite addition (duplicate samples), pre-incubation slurries ($^{13}\text{CH}_4$ -only control, $^{13}\text{CH}_4$ + hematite) and their respective initial slurries (t0) by using the DNeasy PowerLyzer PowerSoil Kit (QIAGEN). Genomic DNA was eluted using 50 μl of elution buffer and stored at -20°C . Metagenomics libraries were prepared at the sequencing core facility at the University of Illinois at Chicago using the Nextera XT DNA library preparation kit (Illumina, USA). Between 19 and 40 million 2×150 bp paired-end reads per library were sequenced using Illumina NextSeq500. Metagenomes were co-assembled from the concatenated reads of all of the metagenomic libraries with Spades V3.12 (Bankevich et al., 2012; Nurk et al., 2013) after decontamination, quality filtering (QV= 10) and adapter-trimming with the BBDuk tool from the BBMap suite (Bushnell B, <http://sourceforge.net/projects/bbmap/>). Downstream analyses, including reading coverage estimates, automatic binning with maxbin (Wu et al., 2014) and metatbat2 (Kang et al., 2019) bin refining with the DAS tool (Sieber et al., 2018), were performed within the SqueezeMeta framework (Tamames and Puente-Sánchez, 2019). GTDB-Tk was used to classify the metagenome-assembled genomes (MAGs) based on Genome Taxonomy Database release 95 (Parks et al., 2021). The principal component analysis biplot was constructed with Past V4.03 (Hammer et al., 2001).

2.3.4 Rate calculations

Methanogenesis rates were calculated from temporal changes in methane concentration in a representative pre-incubated slurry experiment (Fig. 2). The amount of methane oxidized was calculated by a simple mass balance calculation according to equations 1 and 2:

$$x \times F^{13}\text{CH}_4 + (1 - x) \times \text{FDI}^{13}\text{C}_i = \text{FDI}^{13}\text{C}_f \quad (1)$$

$$[\text{CH}_4]_{\text{ox}} = x \times [\text{DIC}]_f \quad (2)$$

The final DIC pool comprises two end members, the initial DIC pool and the oxidized ^{13}C - CH_4 . The term x denotes the fraction of oxidized ^{13}C - CH_4 , while $1-x$ denotes the fraction of the initial DIC pool out of the final DIC pool. $F^{13}\text{CH}_4$ is the fraction of ^{13}C out of the total CH_4 at t0 (i-initial), $\text{FDI}^{13}\text{C}_i$ is the fraction of ^{13}C out of the total DIC at t0, and $\text{FDI}^{13}\text{C}_f$ is the fraction of ^{13}C out of the total DIC at t-final. $[\text{CH}_4]_{\text{ox}}$ is the amount (concentration in pore water) of the methane oxidized throughout the full incubation period, and $[\text{DIC}]_f$ is the DIC concentration at t-final. It was assumed that the isotopic composition of the labeled CH_4 did not change significantly throughout the incubation period.

3. Results

In ten sets of slurry incubation experiments, we followed the progress of the methane oxidation process in Lake Kinneret methanogenic sediments in type A two-stage long-term incubations. This is by monitoring the changes in $\delta^{13}\text{C}_{\text{DIC}}$ values and by running metagenomic and specific isotope lipid

analyses. We also followed methane oxidation in a semi-continuous bioreactor system (type B) with freshly collected sediments with or without the addition of hematite (Fig. 3). The results were compared to those of fresh batch slurry incubations (type C) from the same methanogenic zone, presented by Bar-Or et al. (2017) and Elul et al. (2021).

3.1 Geochemical trends in the long-term two-stage experiments

In the second stage (1:3 ratio of sediment to porewater) long-term batch slurry experiments (type A) from the methanogenic zone, methanogenesis occurred with net methanogenesis rates of $\sim 25 \text{ nmol g dry weight (DW)}^{-1} \text{ d}^{-1}$ (Fig. 2, Table S2), which are similar to those of fresh incubation experiments (Bar-Or et al., 2017). At the same time there was a conversion of ^{13}C -methane to ^{13}C -DIC in all the non-killed slurries amended with ^{13}C -methane, indicating ~~significant~~-AOM (Figs. 3 and 4). The $\delta^{13}\text{C}_{\text{DIC}}$ values of the “methane-only” control slurries reached as high values as 743‰. The average AOM rate in the methane-only controls was $2.0 \pm 0.4 \text{ nmol g DW}^{-1} \text{ d}^{-1}$ (Table 2). AOM was observed in these geochemical experiments also with the addition of electron acceptors, and the potential of several electron acceptors to perform and stimulate the AOM process is detailed below.

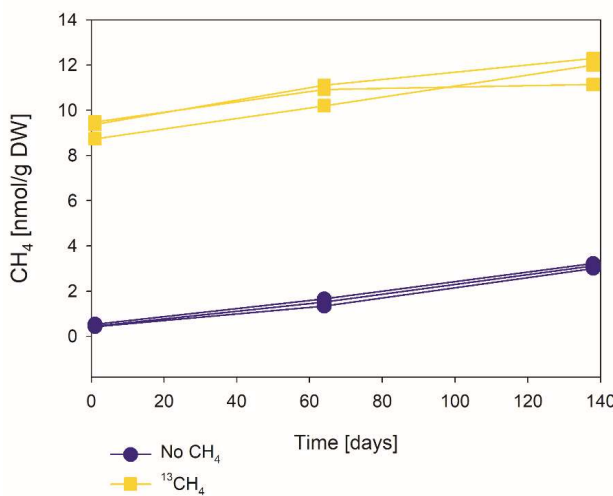


Figure 2: The change of methane concentrations with the time of a representative incubated second stage long-term slurry experiment, showing apparent net methanogenesis with the average rate of $25 \text{ nmol g DW}^{-1} \text{ d}^{-1}$.

3.1.1 Metals as electron acceptors

Iron and manganese oxides were added as potential electron acceptors to the ~~second-second~~-stage long-term slurries. The addition of hematite to three different experiments increased the $\delta^{13}\text{C}_{\text{DIC}}$ values over time to 694‰, similar to the behavior of the methane-only controls, and in a different pattern than the fresh experiments (Fig. 3). The average AOM rate in those two-stage treatments was $1.0 \pm 0.3 \text{ nmol g DW}^{-1} \text{ d}^{-1}$ (Table 3). Magnetite amendments resulted in a minor increase of $\delta^{13}\text{C}_{\text{DIC}}$ values compared to

the methane-only controls (200‰ and 265‰, respectively, Fig. 4A) with an AOM rate of 1.8 nmol g DW⁻¹ d⁻¹. Amorphous iron amendments resulted in only a 22‰ increase in $\delta^{13}\text{C}_{\text{DIC}}$ and a lower AOM rate (0.1 nmol g DW⁻¹ d⁻¹, Fig. 4A and Table 2). The addition of iron-bearing clay nontronite did not cause any increase in the $\delta^{13}\text{C}_{\text{DIC}}$ values (Fig. 4B), but the concentration of dissolved Fe(II) increased compared to the natural methane-only control (Fig. 5). Based on $\delta^{13}\text{C}_{\text{DIC}}$ estimates, no AOM was detected 200 days after the addition of MnO₂ whereas the $\delta^{13}\text{C}_{\text{DIC}}$ values of the methane-only controls increased to over 500‰ (Fig. 4F).

3.1.2 Sulfate as an electron acceptor

The involvement of sulfate in the AOM in the incubations was tested, even in the absence of detectable sulfate in the methanogenic sediments. This is as sulfate could theoretically still be a short living intermediate for the AOM process in an active cryptic sulfur cycle (Holmkvist et al., 2011). It was quantified directly by adding Na-molybdate to the methane-only controls and the magnetite amended treatments with magnetite in the second stage long-term incubations (Fig. 4A). Theis addition of Na-molybdate did not affect the increasing trend of $\delta^{13}\text{C}_{\text{DIC}}$ with time, and therefore, the AOM rates remained unchanged, similar to the observation in the fresh batch incubations (Bar-Or et al., 2017).

3.1.3 Nitrate and nitrite as electron acceptors

Nitrate and nitrite involvement in the AOM was tested for the feasibility of an active cryptic nitrogen cycle, even in the absence of detectable amounts of nitrate and nitrite in the sediments (Nüsslein et al., 2001; Sivan et al., 2011). Nitrate was added at two different concentrations (0.2 and 1 mM, Fig. 4C) to the second stage long-term slurries amended with hematite, as these concentrations were shown previously to promote AOM in other settings (Ettwig et al., 2010). The addition of hematite alone increased the $\delta^{13}\text{C}_{\text{DIC}}$ values by ~200‰ during the 306 days of the experiment. The $\delta^{13}\text{C}_{\text{DIC}}$ in the bottles with the addition of 1 mM nitrate, with and without hematite (Fig. 4C; the data points of the two treatments are on top of each other), decreased from 43‰ at the beginning of the experiment to 35‰ after 306 days. The $\delta^{13}\text{C}_{\text{DIC}}$ in the bottles with the addition of 0.2 mM nitrate and hematite increased by 27‰ at the end of the experiment. Following the addition of 0.5 mM of nitrite, we observed no increase in $\delta^{13}\text{C}_{\text{DIC}}$ values during the first 222 days (Fig. 4D), after which they increased from 34‰ to 54‰ by the end of the experiment. The AOM rate of the high nitrite concentration treatment was 0.2 nmol g DW⁻¹ d⁻¹ (Table 2). Following the addition of 0.1 mM nitrite, $\delta^{13}\text{C}_{\text{DIC}}$ increased only after 130 days to 158‰ on day 493. The AOM rate of the low nitrite concentration treatment was 0.5 nmol g DW⁻¹ d⁻¹. In the methane-only controls, the $\delta^{13}\text{C}_{\text{DIC}}$ value reached a maximum of 330‰.

3.1.4 Organic compounds as electron acceptors

Two of the second stage long-term incubation experiments were amended with synthetic and natural organic electron acceptors to test the potential of organic electron acceptors. The addition of AQDS to slurries with and without hematite caused a decrease in $\delta^{13}\text{C}_{\text{DIC}}$ values over the entire duration of the experiment (Fig. 4E). Dissolved Fe(II) increased by 50 μM in these treatments, while in those without AQDS, it exhibited an increase of 20 μM (Fig. S3). We further tested the effect of naturally occurring humic substances by using those isolated from a different natural lake. The results show that the $\delta^{13}\text{C}_{\text{DIC}}$ values did not change at the beginning of the experiments (Fig. 4B), while a steep increase of ~ 90 μM in their Fe(II) concentration was observed (Fig. 5). After 20 days, the $\delta^{13}\text{C}_{\text{DIC}}$ values of these slurries started to increase dramatically from 84‰ to 150‰ with an AOM rate of 1.2 nmol g DW⁻¹ d⁻¹ (Fig. 4B, Table 2). Dissolved Fe(II) concentrations mirrored the trend of $\delta^{13}\text{C}_{\text{DIC}}$ with a steep increase during the first 20 days followed by a decrease of 37 μM (Fig. 5).

3.1.5 Metabolic pathways

To elucidate which metabolic processes drive AOM, we analyzed $\delta^{13}\text{C}_{\text{DIC}}$ following the addition of inhibitors to the second stage long-term slurries: i) BES, a specific inhibitor for methanogenesis (Nollet et al., 1997) and ii) acetylene, a non-specific inhibitor for methanogenesis and methanotrophy (Oremland and Capone, 1988). In both cases and similar to the killed control, labeled ^{13}C -DIC production was completely inhibited following the addition (Fig. 6). Though acetylene can also inhibit nitrogen cycling in some cases, it has been shown to result in the production of ethylene (Oremland and Capone, 1988). In our case, however, no ethylene was detected, supporting the conclusion that only the methanogenesis activity was inhibited.

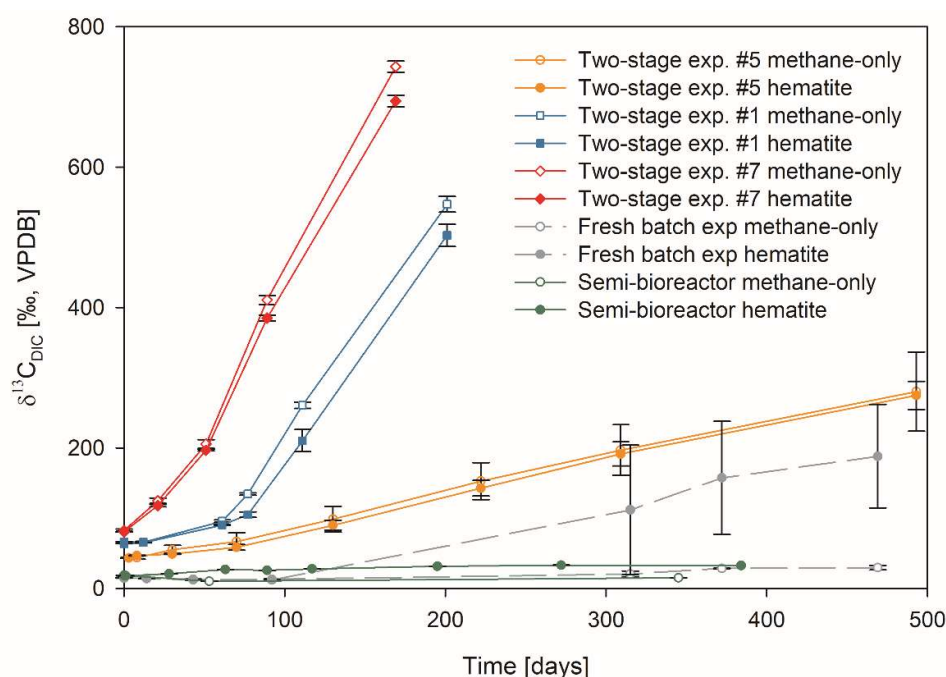


Figure 3: Comparison of $\delta^{13}\text{C}_{\text{DIC}}$ values among the three types of experiments with ^{13}C -labeled methane addition: A) three two-stage slurry experiments (at the second stage of 1:3 ratio of sediment to porewater); B) the semi-continuous bioreactor experiment; and C) slurry batch experiment with freshly collected sediments (Bar-Or et al., 2017). In each experiment, two treatments are shown, with hematite (filled symbol) and without hematite (empty symbols). The error bars represent the average deviation of the mean of duplicate/triplicate bottles.

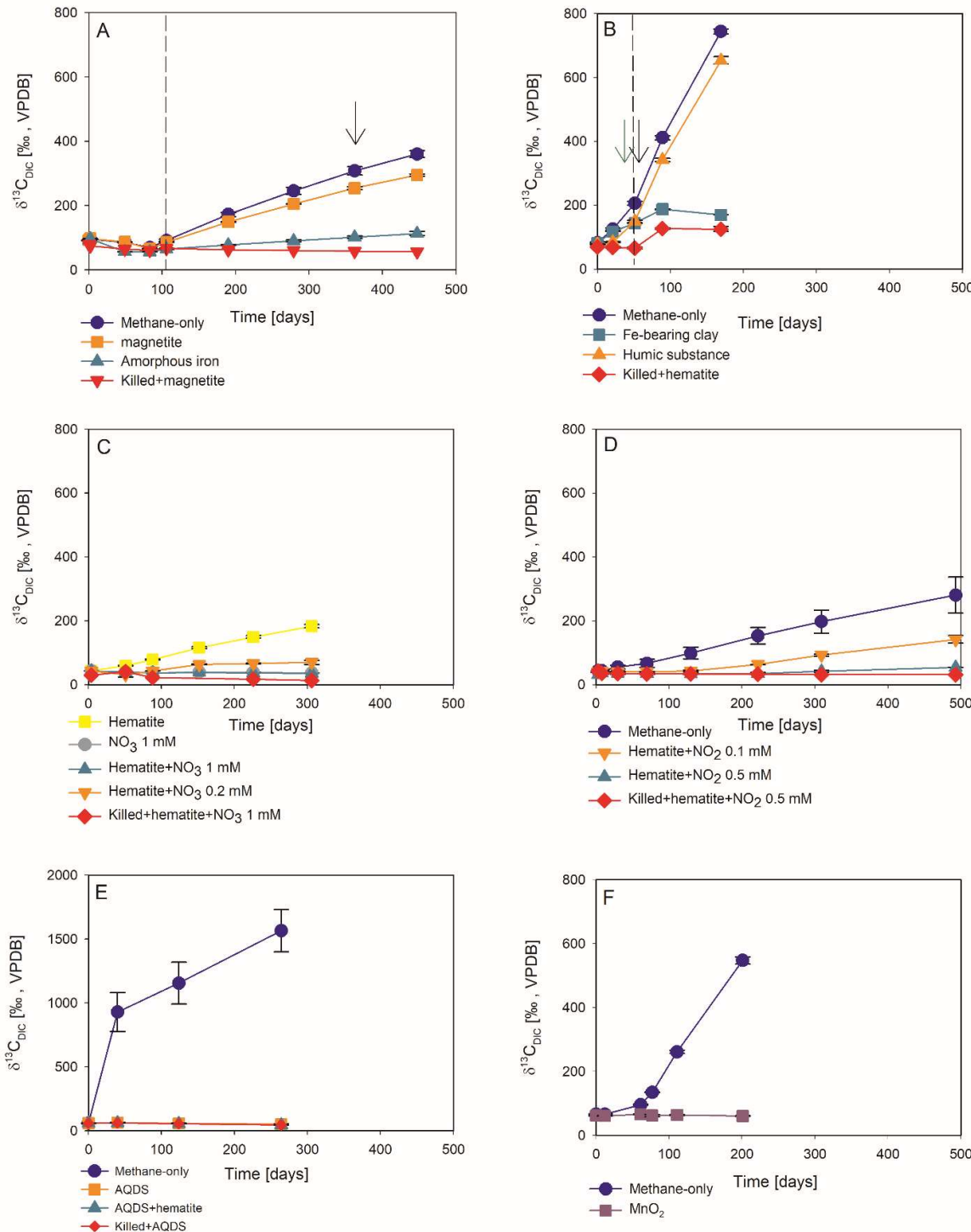


Figure 4: Potentials of different electron acceptors for AOM in Lake Kinneret in the two-stages long-term slurry experiments (at the second stage of 1:3 ratio of sediment to porewater) with of ^{13}C -labeled methane and the following treatments: (A) with and without the addition of magnetite and amorphous iron ($\text{Fe}(\text{OH})_3$). The dashed line represents the specific time of ^{13}C -labeled methane addition. The black arrow represents the addition of Na-molybdate as an inhibitor for sulfate reduction. (B) with clay and natural humic substance. The green arrow represents the time clay was added to the relevant bottles, the dashed line represents the time the headspace of each bottle was flushed again with N_2 , and the black arrow represents the second injection of 1 mL of ^{13}C -labeled methane. (C) with the addition of hematite and two different concentrations of nitrate. (D) with the addition of hematite and two different concentrations of nitrite. (E) with the addition of AQDS. (F) with and without the addition of ^{13}C -labeled methane to ~~all of~~ all the bottles (see Table 1 for specific experimental details). Error bars represent the average deviations of the data points from their means of duplicate/triplicate bottles.

Table 2: AOM rates and AOM role in experiment type A second stage slurries amended with ^{13}C -labeled methane and different electron acceptors (assuming methanogenesis rate of $24.8 \text{ nmol g DW}^{-1} \text{ d}^{-1}$).

Experiment serial number (SN)	Treatment	AOM rate [nmol/g DW X d]	AOM/methanogenesis [%]
10	methane only	1.1	4.4
1	methane only	1.6	6.4
	methane+hematite	0.5	2.1
2	methane only	2.4	8.2
	methane+magnetite	1.8	6.3
	methane+amorphous iron	0.1	0.5
7	methane only	1.4	6.4
	methane+hematite	1.3	6.0
	methane+humics	1.2	5.4
5	methane only	1.0	4.6
	methane+hematite	1.0	4.6
	methane+hematite+nitrite 0.5 mM	0.2	0.8
	methane+hematite+nitrite 0.1 mM	0.5	2.1

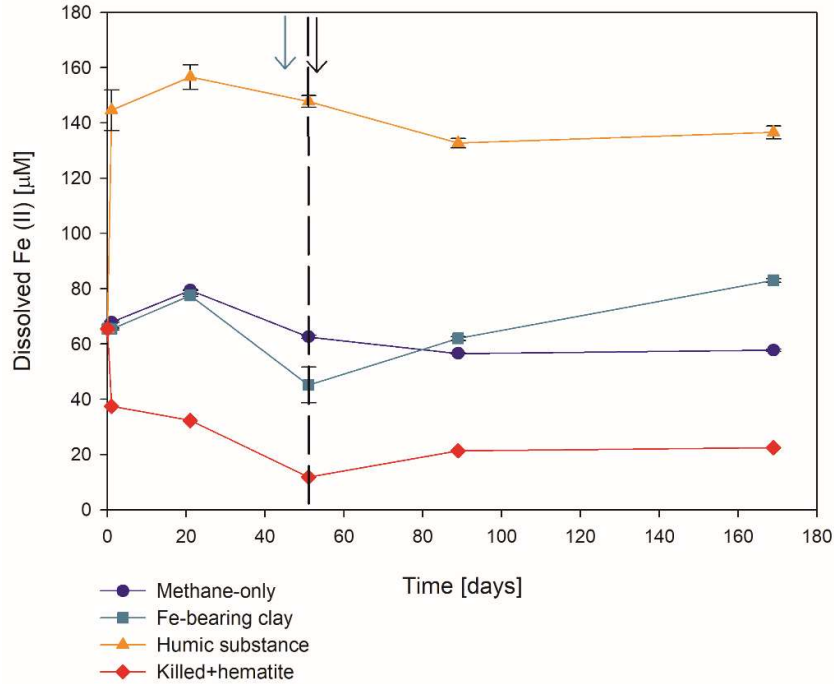


Figure 5: Change in dissolved Fe(II) in the second stage of experiment No. 7 containing clay and natural humic acid. The green arrow represents the time at which clay was added to the specific bottles and those bottles were flushed with N₂, the dashed line represents the time at which the rest of the bottles were flushed, and the black arrow represents the time at which ¹³C-labeled methane was added again. Error bars represent the average of the absolute deviations of the data points from their means.

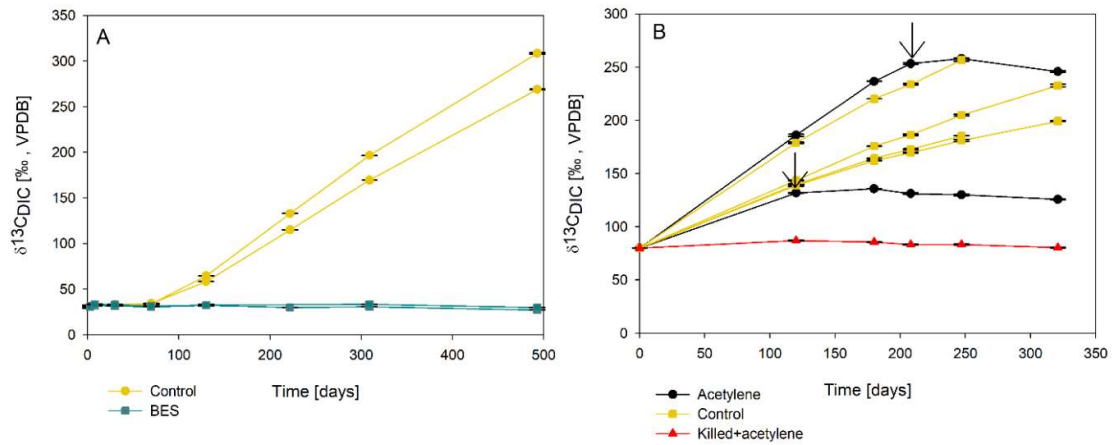


Figure 6: Change in $\delta^{13}\text{C}_{\text{DIC}}$ values over time in the second stage long-term sediment slurry incubations amended with hematite and ¹³C-labeled methane. (A) with/without BES and (B) with/without acetylene. Black arrows represent the time at which acetylene was injected into the experiment bottle. The error bars are smaller than the symbols.

3.2 Microbial dynamics

Analyses of taxonomy and coverage of metagenome-assembled genomes suggest that in the pre-incubated two-stage slurries, Bathyarchaeia are the dominant archaea, together with putative methanogens such as Methanofastidiales (Thermococci), Methanoregulaceae (Methanomicrobia) and Methanotrichales (Methanosarcina) (Supplementary coverage table). Bona-fide ANME (ANME-1) were detected with substantial coverage of approximately 1 (the 27th most abundant from among the 195 MAGs detected) in all of the treatments. Among the bacteria, the sulfate reducers Desulfobacterota and Thermodesulfobivibrionales (Nitrospirota) were prominent together with the GIF9 Dehalococcoida lineage, which is known to metabolize chlorinated compounds in lake sediments (Biderre-Petit et al., 2016). Some Methyloirabilales (NC10) were found (average coverage of 0.32 ± 0.06), and no Methanoperedens were detected. Methylococcales methanotrophs were found in the natural sediments and the fresh batch and bioreactor incubations (average of 0.34 ± 0.02), in contrast to their average coverage of 0.09 ± 0.04 in the long-term incubations. Methylococcales comprised the *Methyloiricola*, *Methyloiramonas* and *Methylobacter* genera (Supplementary coverage table). The methylotrophic partners of aerobic methanotrophs, *Methyloiramonas*, were found in fresh batch and bioreactor incubations, where *Methyloiramonas* was found, findings that are in line with those of previous studies that showed their association (Beck et al., 2013). Principal component analysis shows the grouping of long-term, pre-incubated slurries, semi-aerobic bioreactor incubations, and fresh batch experiments (Fig. 7), emphasizing the microbial dynamics over time.

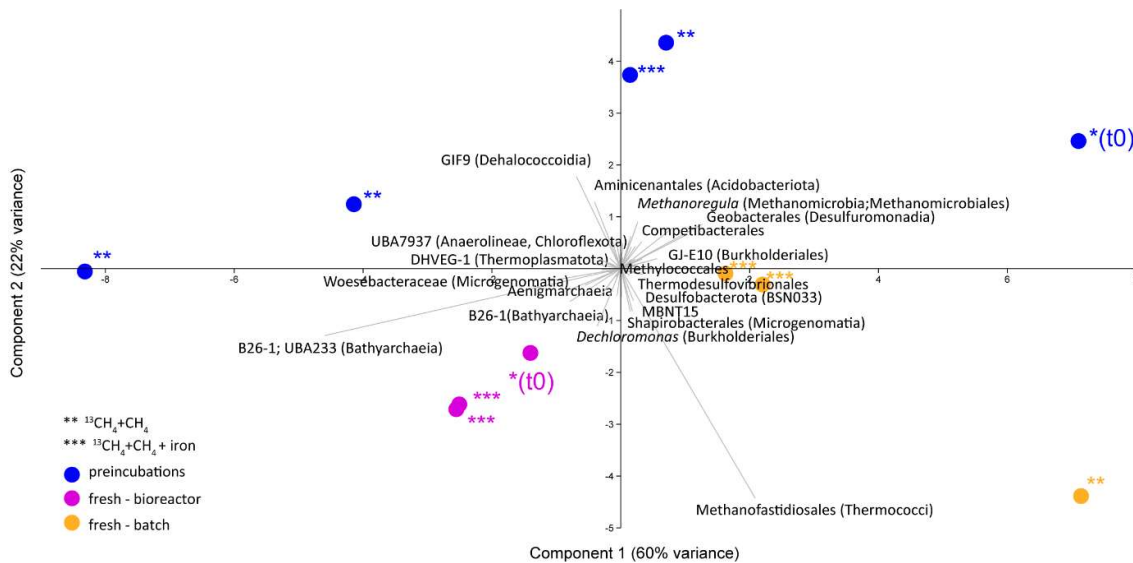


Figure 7: Principal component analysis comparison of three types of samples: long-term pre-incubated slurries (blue – experiment A), semi-continuous bioreactor (pink – experiment B) and fresh batch experiments (orange – experiment C). One asterisk represents t0, two asterisks denote methane-only treatments, three asterisks represent hematite treatment.

3.3 Lipid analysis

The $\delta^{13}\text{C}$ values of the archaeol-derived isoprenoid phytane were between -5 and -17‰ in the long-term pre-incubated samples and thus showed ^{13}C -enrichment of 15 to 27% relative to the original sediment. This is indicative of methane-derived carbon assimilation by archaea (Table 3). Acyclic biphytane, derived mainly from caldarchaeol, exhibited a less pronounced ^{13}C -enrichment of 5-10%. For bacterial-derived fatty acids, $\delta^{13}\text{C}$ -values similarly shifted by up to 10% relative to the original sediment. Nonetheless, one would have expected **much higher** values ~~to be extremely higher~~ if aerobic methanotrophs were active, as was previously indicated by strong ^{13}C -enrichments of up to 1,650% in $\text{C}_{16:1\omega5c}$ observed in freshly incubated batch samples (Bar-Or et al., 2017).

Table 3: The $\delta^{13}\text{C}$ values (in ‰) of fatty acids and isoprenoid hydrocarbons from different experiments compared to values obtained from the original sediment in the methanogenic zone.

Description	Temperature (°C)	Sampling (days)	Fatty acids		Hydrocarbons	
			$\text{C}_{16:1\omega9/8/7}$	$\text{C}_{16:1\omega5}$	Phytane	Biphytane
Pre-incubated slurry + $^{13}\text{CH}_4$ +hematite	20	411	-40	-43	-17	-23
Pre-incubated slurry + $^{13}\text{CH}_4$ (bottle A)	20	411	-40	-43	-13	-24
Pre-incubated slurry + $^{13}\text{CH}_4$ (bottle B)	20	1227	-36	-41	-5	-38
^a Fresh batch experiment+ $^{13}\text{CH}_4$ +hematite	20	470	610	1600	-14	-28
Semi-bioreactor+ $^{13}\text{CH}_4$ +hematite	16	382	n.d.	n.d.	n.d.	n.d.
Original sediment (28-30 cm)	14		-44	-51	-32	-33

^a Bar-Or et al., 2017
n.d. – Not detected

4. Discussion

4.1 Anaerobic oxidation of methane in the methanogenic sediment incubation experiments

The *in-situ* geochemical and microbial diversity profiles (Bar-Or et al., 2015) and the geochemical (Sivan et al., 2011; Bar-Or et al., 2017; Fig. 3) and metagenomic (Elul et al., 2021) analyses of batch incubations with fresh sediments provided strong support for the occurrence of Fe-AOM in sediments of the methanogenic zone below 20 cm. Such profiles and alongside incubations showed an unexpected presence of aerobic bacterial methanotrophs together with anaerobic microorganisms, such as methanogens and iron reducers (Adler et al., 2011; Sivan et al., 2011; Bar-Or et al., 2015; Bar-Or et al., 2017; Elul et al., 2021). These findings suggested that both *mcr* gene-bearing archaea and aerobic bacterial methanotrophs mediate methane oxidation. In the current study, we have supportive evidence of considerable AOM in the long-term incubations, even after the two treatment stages and considering the low abundance of the microbial populations.

The data from the second stage incubations show a similar increasing trend in the $\delta^{13}\text{C}_{\text{DIC}}$ values of both natural (methane-only) and the hematite amended treatments (Fig. 3). This deviates from our observations during experiments B and C with fresh sediment, wherein higher $\delta^{13}\text{C}_{\text{DIC}}$ values were

obtained after the addition of hematite than in the methane-only treatment (Fig. 3 and Bar-Or et al. (2017)). This was particularly dramatic in the batch slurries (experiment C), but it was also observed in the semi-continuous bioreactor (experiment B). We assume that the observed difference in the bioreactors would have been more pronounced if methane concentrations had been higher, but it is still a significant-relevant finding. We also note that the difference between the bioreactors results may also be due to the fact that each bioreactor community developed separately. The results of the type A experiments (compared to those of types B and C) suggest that either hematite lacks the potential to stimulate the AOM activity during the two-stage experiments or that there is enough natural Fe(III) in the sediments to sustain the maximum potential of Fe-AOM. Below we characterize the AOM process in the long-term, two-stage incubation experiments.

4.2 Potential electron acceptors for AOM in the long-term two-stage incubation experiments

4.2.1 Metal oxides as electron acceptors

Measurements of $\delta^{13}\text{C}_{\text{DIC}}$ show that the additions of magnetite, amorphous iron, clays and manganese oxide in the second stage incubations resulted in a less pronounced increase in the $\delta^{13}\text{C}_{\text{DIC}}$ values compared to those of the methane-only controls (Fig. 4). A possible explanation for the latter may be that these metal oxides inhibit AOM, either directly or via a preference for organoclastic iron reduction over Fe-AOM, which adds a natural, more negative carbon isotope signal from the organic materials rather than the heavy carbon from the ^{13}C -labeled methane. Using mass-balance estimations in the methane-only and in the amorphous iron treatments and considering the DIC concentrations and $\delta^{13}\text{C}_{\text{DIC}}$ values of the methane-only treatments at the beginning of the experiment (6 mM and 60‰, respectively) and the values at the end (6.5 mM and 360‰, respectively), about 0.5 mM of the DIC was added by the AOM of methane with $\delta^{13}\text{C}$ of ~4000‰. The DIC and $\delta^{13}\text{C}_{\text{DIC}}$ values of the amorphous iron treatment at the beginning of the experiment were 5.4 mM and 60‰, respectively, and by the end were 6.1 mM and 120‰, respectively. Assuming the same $\delta^{13}\text{C}$ of the added methane of 4000‰ and a $\delta^{13}\text{C}_{\text{TOC}}$ of -30‰ (Sivan et al., 2011), 0.1 mM of the DIC should derive from AOM and 0.6 mM from organoclastic metabolism. This means that adding amorphous iron to the system encouraged iron reduction that was coupled to the oxidation of organic compounds other than methane. Intrinsic microbes, particularly the commonly detected ex-deltaproteobacterial lineages such as Geobacterales, may catalyze Fe(III) metal reduction, regardless of AOM (Xu et al., 2021). Manganese oxides are found in very low abundance in Lake Kinneret sediments (0.1 %, Table S1 and Sivan et al., 2011). Thus, their role in metal-AOM is likely minimal.

4.2.2 Sulfate as an electron acceptor

Sulfate concentrations in the methanogenic Lake Kinneret sediments have been below the detection limit in years past, similar to their representation in the natural sediments we used for the incubations

($< 5 \mu\text{M}$, Bar-Or et al., 2015; Elul et al., 2021). Sulfide concentrations have also been reported to be minor ($< 0.3 \mu\text{M}$, Sivan et al., 2011). However, sulfate could theoretically still be a short-lived intermediate for the AOM process, as pyrite and FeS precipitate in the top sediments, and cryptic cycling via pyrite or FeS may replenish the sulfate, thus rendering it available for AOM (Bottrell et al., 2000). The addition of Na-molybdate to the second stage slurries, including those amended with and without magnetite, did not change the $\delta^{13}\text{C}_{\text{DIC}}$ dynamics, which remained similar to those from before the addition of the inhibitor (Fig. 4A). This finding is in line with that in fresh batch sediment slurries (Bar-Or et al., 2017) and suggests that sulfate is not a potent electron acceptor for AOM in this environment. Furthermore, although sulfate-reducing bacteria were abundant, none of the reducers belonged to the known clades of ANME-2d partners, which were connected previously to the Fe-S- CH_4 coupled AOM (Su et al., 2020; Mostovaya et al., 2021).

4.2.3 Nitrogen species as electron acceptors

Nitrate and nitrite concentrations are also undetectable in the porewater of Lake Kinneret sediments (Nüsslein et al., 2001; Sivan et al., 2011), but again may appear as short-lived intermediate products of ammonium oxidation that is coupled to iron reduction (Tan et al., 2021; Ding et al., 2014; Shrestha et al., 2009; Clement et al., 2005). We thus assessed the roles of nitrate and nitrite as electron acceptors in the two-stage slurries. Our results indicate that the addition of nitrate did not promote AOM, likely due to the absence of ANME-2d, which is known to use nitrate (Arshad et al., 2015; Haroon et al., 2013). In the case of nitrite, even low concentrations appeared to delay the increase in $\delta^{13}\text{C}_{\text{DIC}}$ values, suggesting that organoclastic denitrification outcompetes AOM, and despite the occurrence of Methyloirabacteria, the role of nitrite-AOM is not prominent in the two-stage incubations (Figs. 4C, D).

4.2.4 Humic substances as electron acceptors

Humic substances may promote AOM by continuously shuttling electrons to metal oxides (Valenzuela et al., 2019). Though humic substances were not measured directly in Lake Kinneret sediments, the DOC concentrations in the methanogenic depth porewater were previously found to be high ($\sim 1.5 \text{ mM}$, Adler et al., 2011), suggesting that they may play a role in AOM. Compared to the methane-only treatments, the treatment with the synthetic humic analog AQDS caused an increase in dissolved Fe(II) concentrations, but it did not cause ^{13}C -DIC enrichment. This may be explained by the behavior of AQDS as a strong electron shuttle in organoclastic iron reduction (Lovely et al., 1996), which produces isotopically more negative carbon that masks the AOM signal (Fig. 4E, Fig. S3). Yet, as was done by Valenzuela et al. (2017), the addition of natural humic substances did promote AOM, compared to the rest of the electron acceptors tested, and may thus support AOM (Fig. 4B). In our incubations, the natural humic substances promoted first the oxidation of organic matter by iron reduction, probably by shuttling electrons from the broad spectrum of organic compounds to natural iron oxides (Figs. 4B and

552 5). When the availability of the iron oxides or the organic matter decreased, humic substances likely
553 took over to facilitate the AOM (Fig. 4B).

554 Overall, the results of our long-term two-stage experiments indicate that sulfate, nitrate, nitrite and
555 manganese oxides do not support AOM in the methanogenic sediments of Lake Kinneret. The candidate
556 electron acceptors for AOM in the long-term experiments are natural humic substances and/or the
557 naturally abundant iron minerals. Future experiments can simulate iron limitation and the involvement
558 of iron oxides in the AOM by removing natural iron oxides from the sediments.

559 4.3 Main microbial players in the long-term two-stage slurries

560 Methane oxidation in the pre-incubated Lake Kinneret sediments is likely mediated by either ANMEs
561 or methanogens, as the addition of BES and acetylene immediately stopped the AOM (Fig. 6) similar
562 to the results of the killed bottles and the BES treatment in the fresh batch experiment (Bar-Or et al.,
563 2017). Apart from methane-metabolizing, acetylene can inhibit nitrogen cycling, which results in
564 ethylene production (Oremland and Capone, 1988). This was not the case in our incubations, as no
565 ethylene was produced. The increase in $\delta^{13}\text{C}$ values in phytane and biphytane (Table 3) also indicates
566 the presence of active archaeal methanogens or ANMEs (Wegener et al., 2008; Kellermann et al., 2012;
567 Kurth et al., 2019).

568 Using the isotopic compositions of specific lipids and metagenomics, we identified a considerable
569 abundance of aerobic methanotrophs and methylotrophs in the fresh sediments, but not in the long-term
570 slurries (Table 3, Fig. 7). In the natural sediments, micro levels (nano molar) of oxygen could be trapped
571 in clays and slowly released to the porewater (Wang et al., 2018). However, if such micro levels of
572 oxygen still existed during the time of the pre-incubation, they were probably already exhausted.
573 Indeed, the results of our specific lipids and metagenomics analyses suggest that the aerobic
574 methanotrophs lineages play only a minor role in the long-term slurries, probably due to complete
575 depletion of the oxygen. The metagenomic data (Fig. 7, Supplementary coverage table) also indicate
576 that Bathyarchaea, which may be involved in methane metabolism (Evens et al., 2015), were enriched
577 in the bioreactor incubations, yet their role in Lake Kinneret AOM remains to be evaluated. We also
578 observed changes in the abundance of bacterial degraders of organic matter and necromass: for example,
579 GIF9 Dehalococcoidia, which can metabolize complex organic materials under methanogenic
580 conditions (Cheng et al., 2019; Hug et al., 2013), were most abundant in the long-term incubations (Fig.
581 7, Supplementary coverage table). Though ANME-1 are likely mediators of AOM in these sediments,
582 methane oxidation via reverse methanogenesis is feasible for some methanogens in Lake Kinneret
583 sediments (Elul et al., 2021).

584 4.4 Mechanism of methane oxidation in the long-term two-stage incubations

Our results indicate net methanogenesis in the two-stage incubation experiments with an average rate of 25 nmol gr⁻¹ ~~dry-sediment-DW~~ day⁻¹ (Fig. 1 and Table S2), which are similar to those from fresh incubation experiments (Bar-Or et al., 2017). This is despite the overall trend of increasing $\delta^{13}\text{C}_{\text{DIC}}$ values, a result representing potential methane turnover (Figs. 3 and 4). A likely explanation for the presence of both signals is an interplay between methane production and oxidation, which is possibly triggered by reversal of the methanogenesis pathway in bonafide ANMEs or certain methanogens (Hallam et al., 2004; Timmers et al., 2017). Due to the overall production of methane and the lack of intense stimulation of AOM by any electron acceptor added, the increase in $\delta^{13}\text{C}_{\text{DIC}}$ values could theoretically result from the occurrence of carbon back flux during methanogenesis, which is feasible in environments that are close to thermodynamic equilibrium (Gropp et al., 2021). To test this, we used DIC mass balance calculations to determine the strength of back flux in our incubations. Based on equations 1 and 2, the observed level of ¹³C-enrichment indicates that 3-8% of the ¹³C-methane should be converted into DIC. These estimates are orders of magnitude higher than the previously reported values of 0.001-0.3% for methanogenesis back flux in cultures (Zehnder and Brock, 1979; Moran et al., 2005), but they are in the same range as the back flux of 3.2 to 5.5% observed in ANME-enrichment cultures (Holler et al., 2011). For the latter, however, modeling approaches from AOM-dominated marine sediment samples and associated ANME enrichment cultures indicated the absence of net methanogenesis (Yoshinaga et al., 2014; Chuang et al., 2019; Meister et al., 2019; Wegener et al., 2021). Thus, it seems unlikely that back flux alone can account for the methane-to-DIC conversion in Lake Kinneret sediments. Moreover, the occurrence of back flux alone in marine methanogenic sediments with similar net methanogenesis rates and abundant methane-metabolizing archaea did not yield considerable ¹³C-enrichment in the DIC pool following sediment incubations (Sela-Adler et al., 2015; Amiel, 2018; Vigderovich et al., 2019; Yorshansky, 2019) (Table S3). It is, therefore, less likely that the observed DIC values in our study were sustained by methanogenesis back flux alone (without an external electron acceptor) than by active AOM, which, in this case, is probably performed by ANME-1 or by methanogens, with the latter that performing reverse methanogenesis to some extent.

Conclusions

The previous results of the geochemical and microbial profiles and together with as well as incubations with the fresh sediments incubations from Lake Kinneret sediment constitute evidence of the occurrence of Fe-AOM in the methanogenic zone. The process is, performed by anaerobic archaeal methanogens and aerobic bacterial methanotrophs, which removes about 10-15% of the methane produced in the lake's sediment (Adler et al., 2011; Sivan et al., 2011). In the current study, we found that after two incubation stages and intensive purging for a prolonged duration, AOM was still significant, consuming 3-8% of the methane produced. However, the abundance of aerobic methanotrophs bacteria abundance decreased and only a Anaerobic archaea (ANME-1 or specific methanogens) appeared to be solely

responsible for ~~the methane turnover in these reduced sediments by reverse methanogenesis. It is performed most likely by ANME-1 or specific methanogens. The AOM was observed in all incubation types and could be a result of carbon back flux, as the methanogenic/AOM pathway is reversible, however, the very high $\delta^{13}\text{C}_{\text{DIC}}$ signal points to a metabolic reaction. Terminal electron acceptors or electron shuttles stimulating Fe-AOM are~~It is most either probably coupled to the reduction of hematite reduction and/or humic substances, as terminal electron acceptors or as electron shuttles stimulating the Fe-AOM. The role of the aerobic methanotrophs, but aerobic, of the order *Methylococcales*, which may oxidize methane were found in the freshly collected sediment experiments, however, their role in these the sediments of Lake remains to be examined as well. Potentially these methanotrophs could be responsible for aerobic methane oxidation, suggesting the presence of undetected trace amounts of oxygen in the lake sediments. The co-occurrence of aerobes and anaerobes in the natural environment may be the result of the presence of undetected trace amounts of oxygen that are trapped at those depths in “nano-niches” or even in mineral layers (Wang et al., 2018). This oxygen portion may not be removed by purging at the beginning of our experiments but is rather slowly used by the methanotrophs for their survival. However, In this study we found that after two incubation stages and intensive purging for a prolonged duration, the aerobic bacteria abundance decreased and only archaea remained active and were involved in the observed methane turnover, consuming 3–8% of the methane produced. Thus, we propose two modes of methanotrophy in Lake Kinneret sediments: i) methane oxidation performed by *Methylococcales* species. This mode was observed only in the incubations with freshly collected sediments (batch or bioreactor). ii) methane oxidation through reverse methanogenesis performed most likely by ANME-1 or specific methanogens. This mode was observed in all incubation types and could be a result of carbon back flux, however, the very high $\delta^{13}\text{C}_{\text{DIC}}$ signal points to a metabolic reaction. This AOM is most probably coupled to the reduction of iron and/or humic substances, as terminal electron acceptors or as electron shuttles stimulating the Fe-AOM.

Competing interests. The authors declare that they have no conflict of interest.

Acknowledgments

We would like to thank B. Sulimani and O. Tzabari from the Yigal Allon Kinneret Limnological Laboratory for their onboard technical assistance. We thank all of O. Sivan's lab members for their help during sampling and especially heartfelt thanks to N. Lotem for the invaluable assistance with the mass balance calculations and the fruitful discussions and to E. Eliani-Russak for her technical assistance. Many thanks to K. Hachmann from M. Elvert's lab for his help during lipid analysis and to J. Gropp for insightful discussions about the back flux. This work was supported by ERC consolidator (818450) and Israel Science Foundation (857-2016) grants awarded to O. Sivan. Funding for M. Elvert was provided by the Deutsche Forschungsgemeinschaft (DFG) under Germany's Excellence Initiative/Strategy through the Clusters of Excellence EXC 309 ‘The Ocean in the Earth System’ (project no. 49926684)

and EXC 2077 ‘The Ocean Floor—Earth’s Uncharted Interface’ (project no. 390741601). Funding for M. Rubin-Blum was provided by the Israel Science Foundation (913/19), the U.S.-Israel Binational Science Foundation (2019055) and the Israel Ministry of Science and Technology (1126). H. Vigderovich was supported by a student fellowship from the Israel Water Authority.

References

- Adler, Michal, Eckert, W., & Sivan, O. (2011). Quantifying rates of methanogenesis and methanotrophy in Lake Kinneret sediments (Israel) using porewater profiles. *Limnology and Oceanography*, 56(4), 1525–1535. <https://doi.org/10.4319/lo.2011.56.4.1525>
- Aepfler, R. F., Bühring, S. I., & Elvert, M. (2019). Substrate characteristic bacterial fatty acid production based on amino acid assimilation and transformation in marine sediments. *FEMS Microbiology Ecology*, 95(10), 1–15. <https://doi.org/10.1093/femsec/fiz131>
- Amiel, N. (2018). *Authigenic magnetite in deep sediments*. MsC thesis, Ben Gurion University of the Negev.
- Arshad, A., Speth, D. R., De Graaf, R. M., Op den Camp, H. J. M., Jetten, M. S. M., & Welte, C. U. (2015). A metagenomics-based metabolic model of nitrate-dependent anaerobic oxidation of methane by Methanoperedens-like archaea. *Frontiers in Microbiology*, 6(DEC), 1–14. <https://doi.org/10.3389/fmicb.2015.01423>
- Bai, Y. N., Wang, X. N., Wu, J., Lu, Y. Z., Fu, L., Zhang, F., Lau, T. C., & Zeng, R. J. (2019). Humic substances as electron acceptors for anaerobic oxidation of methane driven by ANME-2d. *Water Research*, 164, 114935. <https://doi.org/10.1016/j.watres.2019.114935>
- Bankevich, A., Nurk, S., Antipov, D., Gurevich, A. a., Dvorkin, M., Kulikov, A. S., Lesin, V. M., Nicolenko, S. I., Pham, S., Pribelski, A. D., Sirotkin, A. V., Vyahhi, N., Tesler, G., Aleksyev, A. M., & Pevzner, P. a. (2012). SPAdes: A New Genome Assembly Algorithm and Its Applications to Single-Cell Sequencing. *Journal of Computational Biology*, 19(5), 455–477. <https://doi.org/10.1089/cmb.2012.0021>
- Bar-Or, I., Ben-Dov, E., Kushmaro, A., Eckert, W., & Sivan, O. (2015). *Methane-related changes in prokaryotes along geochemical profiles in sediments of Lake Kinneret (Israel) Methane-related changes in prokaryotes along geochemical profiles in sediments of Lake Kinneret (Israel)*. (August). <https://doi.org/10.5194/bg-12-2847-2015>
- Bar-Or, I., Elvert, M., Eckert, W., Kushmaro, A., Vigderovich, H., Zhu, Q., Ben-Dov, E., & Sivan, O. (2017). Iron-Coupled Anaerobic Oxidation of Methane Performed by a Mixed Bacterial-Archaeal Community Based on Poorly Reactive Minerals. *Environmental Science & Technology*, 51, 12293–12301. <https://doi.org/10.1021/acs.est.7b03126>
- Bastviken D. (2009). Methane. In: Likens G.E., ed. *Encyclopedia of Inland waters*, Oxford: Elsevier, 783–805. <http://doi.org/10.1016/B978-012370626-3.00117-4>.

690 Beck, D. A. C., Kalyuzhnaya, M. G., Malfatti, S., Tringe, S. G., del Rio, T. G., Ivanova, N., Lidstrom, M. E., &
691 Chistoserdova, L. (2013). A metagenomic insight into freshwater methane-utilizing communities and
692 evidence for cooperation between the Methylococcaceae and the Methylophilaceae. *PeerJ*, 2013(1), 1–23.
693 <https://doi.org/10.7717/peerj.23>

694 Biderre-Petit, C., Dugat-Bony, E., Mege, M., Parisot, N., Adrian, L., Moné, A., Denonfoux, J., Peyretailade, E.,
695 Debroas, D., Boucher, D., Peyret, P. (2016). Distribution of Dehalococcoidia in the anaerobic deep water
696 of a remote meromictic crater lake and detection of Dehalococcoidia-derived reductive dehalogenase
697 homologous genes. *PLoS ONE*, 11(1), 1–19. <https://doi.org/10.1371/journal.pone.0145558>

698 Boetius, A., Ravensschlag, K., Schubert, C. J., Rickert, D., Widdel, F., Gieseke, A., Amann, R., Jørgensen, B.B.,
699 Witte, U., & Pfannkuche, O. (2000). A marine microbial consortium apparently mediating AOM. *Nature*,
700 407(October), 623–626.

701 Bottrell, S. H., Parkes, R. J., Cragg, B. A., & Raiswell, R. (2000): Isotopic evidence for anoxic pyrite oxidation
702 and stimulation of bacterial sulphate reduction in marine sediments, *J. Geol. Soc. London*, 157, 711–714.
703 <https://doi.org/10.1144/jgs.157.4.711>.

704 Cabrol, L., Thalasso, F., Gandois, L., Sepulveda-Jauregui, A., Martinez-Cruz, K., Teisserenc, R., Tananaev, N.,
705 Tveit, A., Svenning, M. M., & Barret, M. (2020). Anaerobic oxidation of methane and associated
706 microbiome in anoxic water of Northwestern Siberian lakes. *Science of the Total Environment*, 736,
707 139588. <https://doi.org/10.1016/j.scitotenv.2020.139588>

708 Cai, C., Leu, A. O., Xie, G-J., Guo, J., Feng, Y., Zhao, J-X., Tyson, G. W., Yuan, Z., & Hu, S. (2018). A
709 methanotrophic archaeon couples anaerobic oxidation of methane to Fe(II) reduction. *ISME J*, 12, 1929-
710 1939. <http://dx.doi.org/10.1038/s41396-018-0109-x>

711 Cheng, L., Shi, S. bao, Yang, L., Zhang, Y., Dolfing, J., Sun, Y. ge, Liu, L., Li, Q., Tu, B., Dai, L., Shi, Q., &
712 Zhang, H. (2019). Preferential degradation of long-chain alkyl substituted hydrocarbons in heavy oil under
713 methanogenic conditions. *Organic Geochemistry*, 138. <https://doi.org/10.1016/j.orggeochem.2019.103927>

714 Chuang, P. C., Yang, T. F., Wallmann, K., Matsumoto, R., Hu, C. Y., Chen, H. W., Lin, S., Sun, CH., Li, HC.,
715 Wang, Y., & Dale, A. W. (2019). Carbon isotope exchange during anaerobic oxidation of methane (AOM)
716 in sediments of the northeastern South China Sea. *Geochimica et Cosmochimica Acta*, 246, 138–155.
717 <https://doi.org/10.1016/j.gca.2018.11.003>

718 Clement, J-C., Shrestha, J., Ehrenfeld, J. G., & Jaffe, P. R. (2005). Ammonium oxidation coupled to
719 dissimilatory iron reduction under anaerobic conditions in wetland soils. *Soil biology and biochemistry*,
720 37(12), 2323-2328. <http://doi.org/10.1016/j.soilbio.2005.03.027>

721 Conrad, R. (2009). The global methane cycle: Recent advances in understanding the microbial processes
722 involved. *Environmental Microbiology Reports*, 1(5), 285–292. [https://doi.org/10.1111/j.1758-](https://doi.org/10.1111/j.1758-2229.2009.00038.x)
723 [2229.2009.00038.x](https://doi.org/10.1111/j.1758-2229.2009.00038.x)

724 Crowe, S. A., Katsev, S., Leslie, K., Sturm, A., Magen, C., Nomosatryo, S., Pack, M. A., Kessler, J. D.,

- Reeburgh, W. S., Roberts, J. a., González, L., Douglas Haffner, G., Mucci, A., Sundby, B., & Fowle, D. A. (2011). The methane cycle in ferruginous Lake Matano. *Geobiology*, 9(1), 61-78.
<http://doi.org/10.1111/j.1472-4669.2010.00257.x>
- Damgaard, L. R., Revsbech, N. P., & Reichardt, W. (1998). Use of an oxygen-insensitive microscale biosensor for methane to measure methane concentration profiles in a rice paddy. *Applied and Environmental Microbiology*, 64(3), 864-870. <http://doi.org/10.1128/aem.64.3.864-870.1998>
- Dershwitz, P., Bandow, N. L., Yang, J., Semrau, J. D., McEllistrem, M. T., Heinze, R. A., Fonseca, M., Ledesma, J. C., Jennett, J. R., DiSpirito, A. M., Athwal, N. S., Hargrove, M. S., Bobik, T. A., Zischka, H., & DiSpirito, A. A. (2021). Oxygen Generation via Water Splitting by a Novel Biogenic Metal Ion-Binding Compound. *Applied and Environmental Microbiology*, 87(14), 1–14.
<https://doi.org/10.1128/aem.00286-21>
- Ding, L. J., An, X. L., Li, S., Zhang, G. L., & Zhu, Y. G. (2014). Nitrogen loss through anaerobic ammonium oxidation coupled to iron reduction from paddy soils in a chronosequence. *Environmental Science and Technology*, 48(18), 10641-10647. <http://doi.org/10.1021/es503113s>
- Elul, M., Rubin-Blum, M., Ronen, Z., Bar-Or, I., Eckert, W., & Sivan, O. (2021). Metagenomic insights into the metabolism of microbial communities that mediate iron and methane cycling in Lake Kinneret sediments. *Biogeosciences Discussions*, 1–24. <https://doi.org/10.5194/bg-2020-329>
- Elvert, M., Boetius, A., Knittel, K., & Jørgensen, B. B. (2003). Characterization of specific membrane fatty acids as chemotaxonomic markers for sulfate-reducing bacteria involved in anaerobic oxidation of methane. *Geomicrobiology Journal*, 20(4), 403–419. <https://doi.org/10.1080/01490450303894>
- Ettwig, K. F., Zhu, B., Speth, D., Keltjens, J. T., Jetten, M. S. M., & Kartal, B. (2016). Archaea catalyze iron-dependent anaerobic oxidation of methane. *PNAS*, 113(45), 12792-12796.
<http://doi.org/10.1073/pnas.1609534113>
- Ettwig, Katharina F, Butler, M. K., Le Paslier, D., Pelletier, E., Mangenot, S., Kuypers, M. M. M., Schreiber, F., Dutilh, B. E., Zedelius, J., de Beer, D., Gloerich, J., Wessels, H. J. C. T., van Alen, T., Luesken, F., Wu, M. L., van de Pas-Schoonen K. T., Op den Camp, H. J. M., Jansen-Megens, E. M., Francoijs, KJ., Stunnenberg, H., Weissenbach, J., Jetten, M. S. M., & Strous, M. (2010). Nitrite-driven anaerobic methane oxidation by oxygenic bacteria. *Nature*, 464(7288), 543–548.
<https://doi.org/10.1038/nature08883>
- Evans, P. N., Parks, D. H., Chadwick, G. L., Robbins, S. J., Orphan V. J., Golding, S. D., & Tyson, G. W. (2015). *Science*. 350(6259), 434-438. <http://doi.org/10.1126/science.aac7745>.
- Fan, L., Dippold, M. A., Ge, T., Wu, J., Thiel, V., Kuzyakov, Y., & Dorodnikov, M. (2020). Anaerobic oxidation of methane in paddy soil: Role of electron acceptors and fertilization in mitigating CH₄ fluxes. *Soil Biology and Biochemistry*, 141, 107685. <https://doi.org/10.1016/j.soilbio.2019.107685>
- Froelich, P. N., Klinkhammer, G. P., Lender, M. L., Luedtke, N. A., Heath, G. R., Cullen, D., Dauphin, P., Hammond, D., Hartman, B., & Maynard, V. (1979). *Geochimica et Cosmochimica Acta*, 43, 1075-1090.
[https://doi.org/10.1016/0016-7037\(79\)90095-4](https://doi.org/10.1016/0016-7037(79)90095-4)
- Gropp, J., Iron, M. A., & Halevy, I. (2021). Theoretical estimates of equilibrium carbon and hydrogen isotope

764 effects in microbial methane production and anaerobic oxidation of methane. *Geochimica et*
765 *Cosmochimica Acta*, 295, 237–264. <https://doi.org/10.1016/j.gca.2020.10.018>

766 Hallam, S. J., Putnam, N., Preston, C. M., Detter, J. C., Rokhsar, D., Richardson, P. H., & DeLong, E. F. (2004).
767 Reverse methanogenesis: Testing the hypothesis with environmental genomics. *Science*, 305(5689),
768 1457–1462. <https://doi.org/10.1126/science.1100025>

769 Hammer, Ø., Harper, D. A. T., & Ryan, P. D. (2001) Past: paleontological statistics software package for
770 education and data analysis. *Paleontologia-Electronica*. 4 (1), 9.
771

772 Haroon, M. F., Hu, S., Shi, Y., Imelfort, M., Keller, J., Hugenholtz, P., Yuan, Z., & Tyson, G. W. (2013).
773 Anaerobic oxidation of methane coupled to nitrate reduction in a novel archaeal lineage. *Nature*,
774 500(7464), 567–570. <https://doi.org/10.1038/nature12375>

775 Hoehler, T. M., Alperin, M. J., Albert, D. B., & Martens, C. S. (1994). Field and laboratory, evidence for a
776 methane-sulfate reducer consortium.pdf. *Global Biogeochemical Cycles*, 8(4), 451–463.

777 Holler, T., Wegener, G., Niemann, H., Deusner, C., Ferdelman, T. G., Boetius, A., Brunner, B., & Widdel, F.
778 (2011). Carbon and sulfur back flux during anaerobic microbial oxidation of methane and coupled sulfate
779 reduction. *Proceedings of the National Academy of Sciences of the United States of America*, 108(52).
780 <https://doi.org/10.1073/pnas.1106032108>

781 Holmkvist, L., Ferdelman, T. G., & Jørgensen, B. B. (2011). A cryptic sulfur cycle driven by iron in the
782 methane zone of marine sediment (Aarhus Bay, Denmark). *Geochimica et Cosmochimica Acta*, 75(12),
783 3581–3599. <https://doi.org/10.1016/j.gca.2011.03.033>

784 Hug, L. A., Castelle, C. J., Wrighton, K. C., Thomas, B. C., Sharon, I., Frischkorn, K. R., Williams, K. H.,
785 Tringe, S. G., & Banfield, J. F. (2013). Community genomic analyses constrain the distribution of
786 metabolic traits across the Chloroflexi phylum and indicate roles in sediment carbon cycling. *Microbiome*,
787 1(1), 1–17. <https://doi.org/10.1186/2049-2618-1-22>

788 Kang, D. D., Li, F., Kirton, E., Thomas, A., Egan, R., An, H., & Wang, Z. (2019). MetaBAT 2: An adaptive
789 binning algorithm for robust and efficient genome reconstruction from metagenome assemblies. *PeerJ*,
790 2019(7), 1–13. <https://doi.org/10.7717/peerj.7359>

791 Kellermann, M. Y., Wegener, G., Elvert, M., Yoshinaga, M. Y., Lin, Y. S., Holler, T., Mollar, P. X., Knittel K.,
792 & Hinrichs, K. U. (2012). Autotrophy as a predominant mode of carbon fixation in anaerobic methane-
793 oxidizing microbial communities. *Proceedings of the National Academy of Sciences of the USA* 109(47),
794 19321–19326. doi:10.1073/pnas.1208795109.

795 Kits, K. D., Klotz, M. G., & Stein, L. Y. (2015). Methane oxidation coupled to nitrate reduction under hypoxia
796 by the Gammaproteobacterium *Methylomonas denitrificans*, sp. nov. type strain FJG1. *Environmental*
797 *Microbiology*, 17(9), 3219–3232. <https://doi.org/10.1111/1462-2920.12772>

798 Knittel, K., & Boetius, A. (2009). Anaerobic oxidation of methane: Progress with an unknown process. *Annual*
799 *Review of Microbiology*, 63, 311–334. <https://doi.org/10.1146/annurev.micro.61.080706.093130>

800 Kurth, J.M., Nadine T Smit, Stefanie Berger, Stefan Schouten, Mike S M Jetten, Cornelia U Welte, Anaerobic
801 methanotrophic archaea of the ANME-2d clade feature lipid composition that differs from other ANME
802 archaea, *FEMS Microbiology Ecology*, Volume 95, Issue 7, July 2019, fiz082.

803 Li, X., Hou, L., Liu, M., Zheng, Y., Yin, G., Lin, X., Cheng, L., Li, Y., & Hu, X. (2015). Evidence of Nitrogen
804 Loss from Anaerobic Ammonium Oxidation Coupled with Ferric Iron Reduction in an Intertidal Wetland.
805 *Environmental Science and Technology*, 49(19), 11560–11568. <https://doi.org/10.1021/acs.est.5b03419>

806 Lin, Y. S., Lipp, J. S., Yoshinaga, M. Y., Lin, S. H., Elvert, M., & Hinrichs, K. U. (2010). Intramolecular stable
807 carbon isotopic analysis of archaeal glycosyl tetraether lipids. *Rapid Communications in Mass*
808 *Spectrometry*, 24(19), 2817–2826. <https://doi.org/10.1002/rcm.4707> Lovley, D. R., & Klug, M. J. (1983).
809 Sulfate reducers can outcompete methanogens at freshwater sulfate concentrations. *Applied and*
810 *Environmental Microbiology*, 45(1), 187–192. <https://doi.org/10.1128/aem.45.1.187-192.1983>

811 Lovely, D. R., Coates, J. D., Blunt-Harris, E. L., Phillips, E. J. P., & Woodward, J. C. (1996). Humic substances
812 as electron acceptors for microbial respiration. *Nature*, 382, 445-448. <https://doi.org/10.1038/382445a0>

813 Lu, Y. Z., Fu, L., Ding, J., Ding, Z. W., Li, N., & Zeng, R. J. (2016). Cr(VI) reduction coupled with anaerobic
814 oxidation of methane in a laboratory reactor. *Water Research*, 102, 445-452.
815 <http://doi.org/10.1016/j.watres.2016.06.065>

816 Martinez-cruz, K., Leewis, M., Charold, I., Sepulveda-jauregui, A., Walter, K., Thalasso, F., & Beth, M. (2017).
817 Science of the Total Environment Anaerobic oxidation of methane by aerobic methanotrophs in sub-
818 Arctic lake sediments. *Science of the Total Environment*, 607–608, 23–31.
819 <https://doi.org/10.1016/j.scitotenv.2017.06.187>

820 Meador, T. B., Gagen, E. J., Loscar, M. E., Goldhammer, T., Yoshinaga, M. Y., Wendt, J., Thomm, M., &
821 Hinrichs, K. U. (2014). Thermococcus kodakarensis modulates its polar membrane lipids and elemental
822 composition according to growth stage and phosphate availability. *Frontiers in Microbiology*, 5(JAN), 1–
823 13. <https://doi.org/10.3389/fmicb.2014.00010>

824 Meister, P., Liu, B., Khalili, A., Böttcher, M. E., & Jørgensen, B. B. (2019). Factors controlling the carbon
825 isotope composition of dissolved inorganic carbon and methane in marine porewater: An evaluation by
826 reaction-transport modelling. *Journal of Marine Systems*, 200(August), 103227.
827 <https://doi.org/10.1016/j.jmarsys.2019.103227>

828 Moran, J. J., House, C. H., Freeman, K. H., & Ferry, J. G. (2005). Trace methane oxidation studied in several
829 Euryarchaeota under diverse conditions. *Archaea*, 1(5), 303–309. <https://doi.org/10.1155/2005/650670>

830 Mosrovaya, A., Wind-Hansen, M., Rousteau, P., Bristow, L. A., & Thamdrup, B. (2021) Sulfate- and iron-
831 dependent anaerobic methane oxidation occurring side-by-side in freshwater lake sediments. *Limnology*
832 *and Oceanography*. <https://doi.org/10.1002/lno.11988>

833 Nollet, L., Demeyer, D., & Verstraete, W. (1997). Effect of 2-bromoethanesulfonic acid and Peptostreptococcus
834 productus ATCC 35244 addition on stimulation of reductive acetogenesis in the ruminal ecosystem by
835 selective inhibition of methanogenesis. *Applied and Environmental Microbiology*, 63(1), 194–200.

836 <https://doi.org/10.1128/aem.63.1.194-200.1997>

837 Norði, K. á., Thamdrup B., & Schubert, C. J. (2013). Anaerobic oxidation of methane in an iron-rich Danish
 838 freshwater lake sediment. *Limnology and Oceanography*, 58(2), 546-554.
 839 <http://doi.org/10.4319/lo.2013.58.2.0546>

840 Norði, K. á., & Thamdrup B. (2014). Nitrate-dependent anaerobic methane oxidation in freshwater sediment.
 841 *Geochimica et Cosmochimica Acta*, 132, 141-150. <http://doi.org/10.1016/j.gca.2014.01.032>

842 Nurk, S., Bankevich, A., & Antipov, D. (2013). Assembling genomes and mini-metagenomes from highly
 843 chimeric reads. *Research in Computational Molecular Biology*, 158–170. [https://doi.org/10.1007/978-3-](https://doi.org/10.1007/978-3-642-37195-0)
 844 [642-37195-0](https://doi.org/10.1007/978-3-642-37195-0)

845 Nüsslein, B., Chin, K. J., Eckert, W., & Conrad, R. (2001). Evidence for anaerobic syntrophic acetate oxidation
 846 during methane production in the profundal sediment of subtropical Lake Kinneret (Israel). *Environmental*
 847 *Microbiology*, 3(7), 460–470. <https://doi.org/10.1046/j.1462-2920.2001.00215.x>

848 Orembland, R. S., & Capone, D. G. (1988). *Use of "Specific" Inhibitors in Biogeochemistry and Microbial*
 849 *Ecology* (Vol. 10). <https://doi.org/10.2307/4514>

850 Orphan, V. J., House, C. H., & Hinrichs, K. (2001). Methane-Consuming Archaea Revealed by Directly
 851 Coupled Isotopic and Phylogenetic Analysis. *Science*, 293(July), 484–488.
 852 <https://doi.org/10.1126/science.1061338>

853 Oswald, K., Milucka, J., Brand, A., Hach, P., Littmann, S., Wehrli, B., Albersten, M., Daims, H., Wagner, M.,
 854 Kuypers, M. M. M., Schubert, C. J., & Milucka, J. (2016). Aerobic gammaproteobacterial methanotrophs
 855 mitigate methane emissions from oxic and anoxic lake waters. *Limnology and Oceanography*, 61, S101–
 856 S118. <https://doi.org/10.1002/lno.10312>

857 Parks, D. H., Chuvochina, M., Rinke, C., Mussig, A. J., Chaumeil, P.-A., & Hugenholtz, P. (2021) GTDB: an
 858 ongoing census of bacterial and archaeal diversity through a phylogenetically consistent, rank
 859 normalized and complete genome-based taxonomy. *Nucleic Acids Research*, 202, 1-10.
 860 <http://doi.org/10.1093/nar/gkab776>

861 Raghoebarsing, A. A., Pol, A., Van De Pas-Schoonen, K. T., Smolders, A. J. P., Ettwig, K. F., Rijpstra, W. I. C.,
 862 Schouten, S., Sinninghe Damsté, J. S., Op den Camp, H. J. M., Jetten, M. S. M., & Strous, M. (2006). A
 863 microbial consortium couples anaerobic methane oxidation to denitrification. *Nature*, 440(7086), 918–
 864 921. <https://doi.org/10.1038/nature04617>

865 Reeburgh, W. S. (2007). Oceanic Methane Biogeochemistry. *ChemInform*, 38(20), 486–513.
 866 <https://doi.org/10.1002/chin.200720267>

867 Rosentreter, J. A., Borges, A. V., Deemer, B. R., Holgerson, M. A., Liu, S., Song, C., Melack, J., Raymond, P.
 868 A., Duarte, C. M., Allen, G. H., Olefeldt, D., Poulter, B., Battin, T. I., & Eyre, B. D. (2021). *Nature*
 869 *geoscience*, 14(4), 225-230. <http://doi.org/10.1038/s41561-021-00715-2>

870 Saunois, M., Stavert, A. R., Poulter, B., Bousquet, P., Canadell, J. G., Jackson, R. B., Raymond, P. A.,

871 Dlugokencky, E. J., Houweling, S., Patra, P. K., Ciais, P., Arora, V. K., Bastviken, D., Bergamaschi, P.,
872 Blake, D. R., Brailsford, G., Bruhwiler, L., Carlson, K. M., Carrol, M., Castaldi, S., Chandra, N.,
873 Crevoisier, C., Crill, P. M., Covey, K., Curry, C. L., Etiope, G., Frankenberg, C., Gedney, N., Hegglin, M.
874 I., Höglund-Isaksson, L., Hugelius, G., Ishizawa, M., Ito, A., Janssens-Maenhout, G., Jensen, K. M., Joos,
875 F., Kleinen, T., Krummel, P. B., Langenfelds, R. L., Laruelle, G. G., Liu, L., Machida, T., Maksyutov, S.,
876 McDonald, K. C., McNorton, J., Miller, P. A., Melton, J. R., Morino, I., Müller, J., Murguia-Flores, F.,
877 Naik, V., Niwa, Y., Noce, S., O'Doherty, S., Parker, R. J., Peng, C., Peng, S., Peters, G. P., Prigent, C.,
878 Prinn, R., Ramonet, M., Regnier, P., Riley, W. J., Rosentreter, J. A., Segers, A., Simpson, I. J., Shi, H.,
879 Smith, S. J., Steele, L. P., Thornton, B. F., Tian, H., Tohjima, Y., Tubiello, F. N., Tsuruta, A., Viovy, N.,
880 Voulgarakis, A., Weber, T. S., van Weele, M., van der Werf, G. R., Weiss, R. F., Worthy, D., Wunch, D.,
881 Yin, Y., Yoshida, Y., Zhang, W., Zhang, Z., Zhao, Y., Zheng, B., Zhu, Q., Zhu, Q., and Zhuang, Q.: The
882 Global Methane Budget 2000–2017, *Earth Syst. Sci. Data*, 12, 1561–1623, [https://doi.org/10.5194/essd-](https://doi.org/10.5194/essd-12-1561-2020)
883 12-1561-2020, 2020.

884 Schubert, C. J., Vazquez, F., Lösekann-Behrens, T., Knittel, K., Tonolla, M., & Boetius, A. (2011). Evidence for
885 anaerobic oxidation of methane in sediments of a freshwater system (Lago di Cadagno). *FEMS*
886 *Microbiology Ecology*, 76(1), 26-38. <http://doi.org/10.1111/j.1574-6941.2010.01036.x>

887 Segarra, K. E. A., Schubotz, F., Samarkin, V., Yoshinaga, M. Y., Hinrichs, K-U., & Joye, S. B. (2015). *Nature*
888 *communications*, 6(may), 1-8. <http://dx.doi.org/10.1038/ncomms8477>

889 Sela-Adler, M., Herut, B., Bar-Or, I., Antler, G., Eliani-Russak, E., Levy, E., Makovsky, Y., & Sivan, O.
890 (2015). Geochemical evidence for biogenic methane production and consumption in the shallow
891 sediments of the SE Mediterranean shelf (Israel). *Continental Shelf Research*, 101, 117–124.
892 <https://doi.org/10.1016/j.csr.2015.04.001>

893 Shrestha, J., Rich, J. J., Ehrenfeld, J. G., & Jaffe, P. R. (2009). Oxidation of ammonium to nitrite under iron-
894 reducing conditions in wetland soils: Laboratory, field demonstrations, and push-pull rate determination.
895 *Soil Science*, 174(3), 156-164. <http://doi.org/10.1097/SS.0b013e3181988fbf>

896 Shuai, W., & Jaffé, P. R. (2019). Anaerobic ammonium oxidation coupled to iron reduction in constructed
897 wetland mesocosms. *Science of the Total Environment*, 648, 984–992.
898 <https://doi.org/10.1016/j.scitotenv.2018.08.189>

899 Sieber, C. M. K., Probst, A. J., Sharrar, A., Thomas, B. C., Hess, M., Tringe, S. G., & Banfield, J. F. (2018).
900 Recovery of genomes from metagenomes via a dereplication, aggregation and scoring strategy. *Nature*
901 *Microbiology*, 3(7), 836–843. <https://doi.org/10.1038/s41564-018-0171-1>

902 Sinke, A. J.C., Cornelese, A. A., Cappenberg, T. E., & Zehnder, A. J. B. (1992). Seasonal variation in sulfate
903 reduction and methanogenesis in peaty sediments of eutrophic Lake Loosdrecht, The Netherlands.
904 *Biogeochemistry*, 16(1), 43-61. <http://doi.org/10.1007/BF02402262>

905 Sivan, O., Adler, M., Pearson, A., Gelman, F., Bar-Or, I., John, S. G., & Eckert, W. (2011). Geochemical
906 evidence for iron-mediated anaerobic oxidation of methane. *Limnology and Oceanography*, 56(4), 1536–
907 1544.

908 Stookey, L. L. (1970). Ferrozine-a new spectrophotometric reagent for iron. *Analytical Chemistry*, 42(7), 779–

781. <https://doi.org/10.1021/ac60289a016>

Sturt, H. F., Summons, R. E., Smith, K., Elvert, M., & Hinrichs, K. U. (2004). Intact polar membrane lipids in prokaryotes and sediments deciphered by high-performance liquid chromatography/electrospray ionization multistage mass spectrometry - New biomarkers for biogeochemistry and microbial ecology. *Rapid Communications in Mass Spectrometry*, 18(6), 617–628. <https://doi.org/10.1002/rcm.1378>

Su, G., Zopfi, J., Yao, H., Steinle, L., Niemann, H., & Lehmann, M. F. (2020). Manganese/iron-supported sulfate-dependent anaerobic oxidation of methane by archaea in lake sediments. *Limnology and Oceanography*, 65(4), 863–875. <https://doi.org/10.1002/lno.11354>

Tamames, J., & Puente-Sánchez, F. (2019). SqueezeMeta, A Highly Portable, Fully Automatic Metagenomic Analysis Pipeline. *Frontiers in Microbiology*, 9. <https://doi.org/10.3389/fmicb.2018.03349>

Tan, X., Xie, G. J., Nie, W. B., Xing, D-F., Liu, B. F., Ding, J., & Ren, N. Q. (2021). Fe(III)-mediated anaerobic ammonium oxidation: A novel microbial nitrogen cycle pathway and potential applications. *Critical Reviews in Environmental Science and Technology*. <https://doi.org/10.1080/10643389.2021.1903788>

Timmers, P. H. A., Welte, C. U., Koehorst, J. J., Plugge, C. M., Jetten, M. S. M., & Stams, A. J. M. (2017). Reverse Methanogenesis and Respiration in Methanotrophic Archaea. *Archaea*, 2017(Figure 1). <https://doi.org/10.1155/2017/1654237>

Treude, T., Krause, S., Maltby, J., Dale, A. W., Coffin, R., & Hamdan, L. J. (2014). Sulfate reduction and methane oxidation activity below the sulfate-methane transition zone in Alaskan Beaufort Sea continental margin sediments: Implications for deep sulfur cycling. *Geochimica et Cosmochimica Acta*, 144, 217–237. <https://doi.org/10.1016/j.gca.2014.08.018>

Treude, T., Niggemann, J., Kallmeyer, J., Wintersteller, P., Schubert, C. J., Boetius, A., & Jørgensen, B. B. (2005). Anaerobic oxidation of methane and sulfate reduction along the Chilean continental margin. *Geochimica et Cosmochimica Acta*, 69(11), 2767–2779. <https://doi.org/10.1016/j.gca.2005.01.002>

Valentine D. L. (2002). Biogeochemistry and microbial ecology of methane oxidation in anoxic environments: A review. *Antonie van Leeuwenhoek*, 81(1-4), 271-282. <http://doi.org/10.1023/A:1020587206351>

Valenzuela, E. I., Avendaño, K. A., Balagurusamy, N., Arriaga, S., Nieto-Delgado, C., Thalasso, F., & Cervantes, F. J. (2019). Electron shuttling mediated by humic substances fuels anaerobic methane oxidation and carbon burial in wetland sediments. *Science of the Total Environment*, 650, 2674–2684. <https://doi.org/10.1016/j.scitotenv.2018.09.388>

Valenzuela, E. I., Prieto-Davó, A., López-Lozano, N. E., Hernández-Eligio, A., Vega-Alvarado, L., Juárez, K., García-González, A. S., López, M. G., & Cervantes, F. J. (2017). Anaerobic methane oxidation driven by microbial reduction of natural organic matter in a tropical wetland. *Applied and Environmental Microbiology*, 83(11), 1–15. <https://doi.org/10.1128/AEM.00645-17>

Vigderovich, H., Liang, L., Herut, B., Wang, F., Wurgaft, E., Rubin-Blum, M., & Sivan, O. (2019). Evidence for microbial iron reduction in the methanogenic sediments of the oligotrophic SE Mediterranean

continental shelf. *Biogeosciences Discussions*, 1–25. <https://doi.org/10.5194/bg-2019-21>

Wang, L., Miao, X., Ali, J., Lyu, T., & Pan, G. (2018). Quantification of Oxygen Nanobubbles in Particulate Matters and Potential Applications in Remediation of Anaerobic Environment. *ACS Omega*, 3(9), 10624–10630. <https://doi.org/10.1021/acsomega.8b00784>

Wegener G, Niemann H, Elvert M, Hinrichs K-U, Boetius A (2008). Assimilation of methane and inorganic carbon by microbial communities mediating the anaerobic oxidation of methane. *Environmental Microbiology* 10(9), 2287-2298. doi: 10.1111/j.1462-2920.2008.01653.x.

Wegener, G., Gropp, J., Taubner, H., Halevy, I., & Elvert, M. (2021). Sulfate-dependent reversibility of intracellular reactions explains the opposing isotope effects in the anaerobic oxidation of methane. *Science Advances*, 7(19), 1–14. <https://doi.org/10.1126/sciadv.abe4939>

Whiticar, M. J., Faber, E., & Schoell, M. (1986). Biogenic methane formation in marine and freshwater environments: CO₂ reduction vs. acetate fermentation-Isotope evidence. *Geochimica et Cosmochimica Acta*, 50(5), 693-709. [http://doi.org/10.1016/0016-7037\(86\)90346-7](http://doi.org/10.1016/0016-7037(86)90346-7)

Wu, Y.W., Tang, Y.-H., Tringe, S. G., Simmons, B. A., & Singer, S. W. (2014). MaxBin: an automated binning method to recover individual genomes from metagenomes using. *Microbiome*, 2(26), 4904–4909. Retrieved from <https://microbiomejournal.biomedcentral.com/articles/10.1186/2049-2618-2-26>

Wuebbles, D. J., & Hayhoe, K. (2002). Atmospheric methane and global change. *Earth-Science Reviews*, 57(3–4), 177–210. [https://doi.org/10.1016/S0012-8252\(01\)00062-9](https://doi.org/10.1016/S0012-8252(01)00062-9)

Xu, Z., Masuda, Y., Wang, X., Ushijima, N., Shiratori, Y., Senoo, K., & Itoh, H. (2021). Genome-Based Taxonomic Rearrangement of the Order Geobacterales Including the Description of *Geomonas azotofigans* sp. nov. and *Geomonas diazotrophica* sp. nov. *Frontiers in Microbiology*, 12(September). <http://doi.org/10.3389/fmicb.2021.737531>

Yorshansky, O. (2019). *Iron Reduction in Deep Marine Sediments of the Eastern Mediterranean Continental Shelf and the Yarqon Estuary*. MsC thesis, Ben Gurion University of the Negev.

Yoshinaga, M. Y., Holler, T., Goldhammer, T., Wegener, G., Pohlman, J. W., Brunner, B., Kuypers, M. M. M., Hinrichs, K. U., & Elvert, M. (2014). Carbon isotope equilibration during sulphate-limited anaerobic oxidation of methane. *Nature Geoscience*, 7(3), 190–194. <https://doi.org/10.1038/ngeo2069>

Zehnder, a J., & Brock, T. D. (1979). Methane formation and methane oxidation by methanogenic bacteria. *Journal of Bacteriology*, 137(1), 420–432.

Zhang, X., Xia, J., Pu, J., Cai, C., Tyson, G. W., Yuan, Z., & Hu, S. (2019). Biochar-Mediated Anaerobic Oxidation of Methane. *Environmental Science and Technology*, 53(12), 6660–6668. <https://doi.org/10.1021/acs.est.9b01345>

Zheng, Y., Wang, H., Liu, Y., Zhu, B., Li, J., Yang, Y., Qin, W., Chen, L., Wu, X., Chistoserdova, L., & Zhao, F. (2020). Methane-Dependent Mineral Reduction by Aerobic Methanotrophs under Hypoxia. *Environmental Science and Technology Letters*, 7(8), 606–612. <https://doi.org/10.1021/acs.estlett.0c00436>

